K_{ATP} Channel blockade instructs microglia to foster brain repair and neurogenesis after stroke

Fco. Javier Ortega González

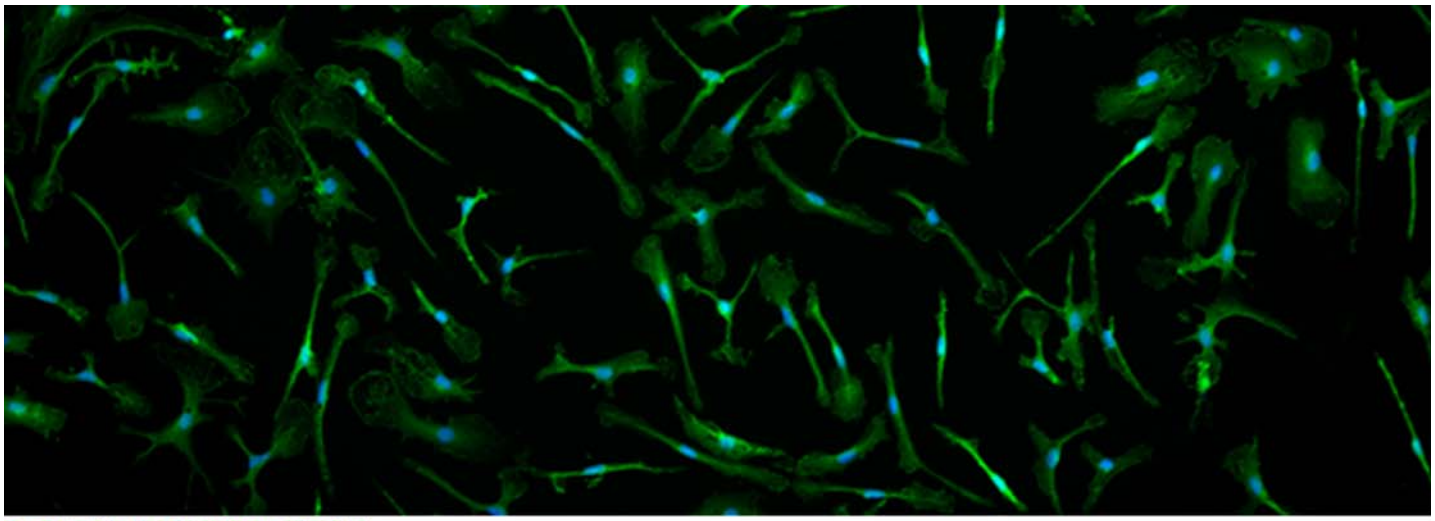

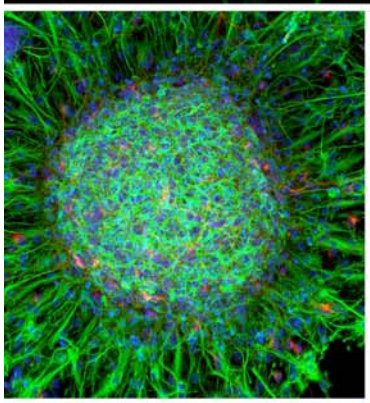

K_{ATP} channel blockade instructs microglia to foster brain repair and neurogenesis after stroke

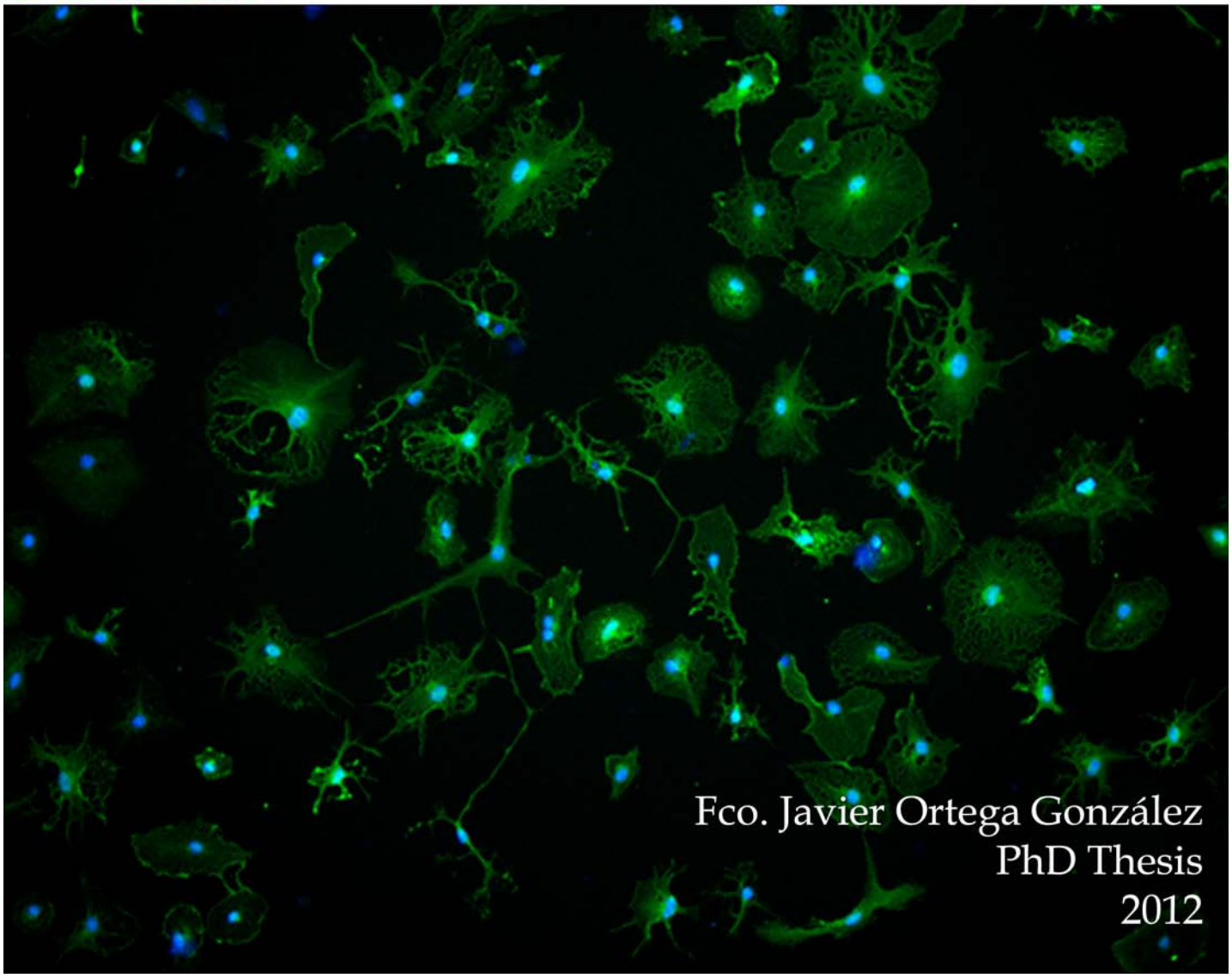

Fco. Javier Ortega González

PhD Thesis

2012

K_{ATP} CHANNEL BLOCKADE INSTRUCTS MICROGLIA TO FOSTER BRAIN REPAIR AND NEUROGENESIS AFTER STROKE

Fco. Javier Ortega González

PhD Thesis

Barcelona, March 2012

Tesi doctoral

K_{ATP} CHANNEL BLOCKADE INSTRUCTS MICROGLIA TO FOSTER BRAIN REPAIR AND NEUROGENESIS AFTER STROKE

Dr. Manuel J. Rodríguez Allué, Professor titular de la Universitat de Barcelona,

CERTIFICA:

Que la següent Tesi Doctoral, presentada per en Fco. Javier Ortega Gonález, Llicenciat en Bioquímica per la Universitat Autònoma de Barcelona, ha estat realitzada sota la seva direcció al Departament de Ciències Fisiològiques I (IDIBAPS), Unitat de Bioquímica, de la Universitat de Barcelona i reuneix tots els requisits necessaris per ser llegida i defensada davant el tribunal corresponent, autoritzant la seva presentació per optar al grau de Doctor en Biomedicina per la Universitat de Barcelona.

El doctorand — El director de la tesi

Fco. Javier Ortega González — Dr. Manuel J. Rodríguez Allué

Barcelona, Març 2012

It is not the strongest of the species that survives,

nor the most intelligent that survives.

It is the one that is the most adaptable to change.

Charles Darwin (1809-1882)

A mi familia,

a todos los que están,

y a los que vuelan libres…

PUBLICACIONS i FINANÇAMENT

El treball aquí presentat ha donat com a fruit les següents publicacions internacionals:

- **Ortega F.J**., Gimeno-Bayon J., Espinosa-Parrilla J.F., Carrasco J.L., Batlle M., Pugliese M., Mahy N., Rodríguez M.J. **ATP-Dependent Potassium Channel Blockade Strengthens Microglial Neuroprotection after Hypoxia-Ischemia in Rats.** Exp Neurol (2012) Feb 24 (*Epub ahead of print*)**.**
  doi: 10.1016/j.expneurol.2012.02.010

- **Ortega F.J**., Jolkkonen J., Mahy N., Rodríguez M.J. **Glibenclamide Enhances Neurogenesis and Improves Long-term Functional Recovery after Transient Focal Cerebral Ischemia.** Stroke (Submitted)

- **Ortega F.J**., Vukovic J., Rodríguez M.J., Bartlett P.F. **Microglial K_{ATP}-channel blockade instructs activation of neural precursors from the subventricular zone.** Glia (Submitted)

- **Ortega F.J.**, Vidal-Taboada J.M., Mahy N., Rodríguez M.J. **Molecular Mechanisms of Acute Brain Injury and Ensuing Neurodegeneration**, Brain Damage - Bridging Between Basic Research and Clinics, Alina González-Quevedo (Ed.), ISBN:978-953-51-0375-2, InTech, Available from: www.intechopen.com/articles/show/title/molecular-mechanisms-of-acute-brain-injury-and-ensuing-neurodegeneration

Aquesta tesi ha estat realitzada gràcies al finançament dels projectes següents:

- Ministerio de Ciencia e Innovación (MICIN). Ref. SAF SAF2008-01902 y PET2007-0450.
- Generalitat de Catalunya, Ref. 2009SGR1380.
- Centre for International Mobility (CIMO), Finland.
- National Health and Medical Research Council program grant and supported by the Estate of Dr Clem Jones AO, Australia.
- F.J.O. ha rebut una beca doctoral FPU del Ministerio de Educación y Ciencia.

Agraïments

En primer lloc m'agradaria agrair a la Dra. Nicole Mahy per donar-me la possibilitat de realitzar la tesis doctoral al seu grup, per haver trobar el finançament que m'ha permès realitzar el meu projecte durant tots aquest anys, i per encoratjar-me a deixar una beca associada a empresa per agafar la FPU. Sense aquesta empenta no hagués estat possible realitzar les dues estades internacionals i emportar-me dues grans experiències tan personals com laborals durant el doctorat.

Al Dr. Manuel J. Rodríguez, tot i que per nosaltres sempre seràs en Manolo... per no només guiar-me durant tot aquest procés, haver tingut xerrades de ciència i trobar un significat a els meus resultats que a vegades jo no ho veia gens clar, sinó també, per ajudar-me a muntar els dos projectes per marxar afora, i amb tots els dubtes existencials que he tingut, sobre tot a la recta final de la tesis. Però sobre tot, i especialment per que m'emporto la sensació que sempre t'he pogut parlar amb tota sinceritat, i crec hem sigut capaços de trencar aquesta barrera de jefe-treballador que a vegades és més un obstacle que no pas un avantatge.

Al **Dr. Marco Pugliese**, por haber formado parte de su equipo de Neurotec, aunque solo fuera por unos meses, y no enfadarse (sólo lo debido) por aceptar la beca FPU y tener que cambiar de proyecto de investigación. También por enseñarme un poco más de italiano, supongo que nunca es suficiente, por cierto, nunca olvidaré una gran frase tuya: "Bene nappa…"

To **Dr. Jukka Jolkonnen** from the Stroke Recovery Laboratory, Kuopio, Finland, for being patient and show me all the behavioral tests, as well as, for sharing with me all the typical Finnish live-style habits, such as, saunas, snow, ice skating over a frozen lake. Also, I'd to thank you that dinner with typical Finnish food and sharing it with your family, that night made me feel like home although we were at -15ºC, hehe. And specially to offer me the chance to go back to Kuopio as a Postdoc, and get definitely into snow sports, and remember my first visit to such a beautiful spot surrounded by nature.

To **Dr. Perry F. Bartlett**, from the Queensland Brain Institute, Brisbane, Australia, for giving me the weekly newsletter about all the events that were going on in BrisVegas, and to suggest me all what I had to visit in Oz befote coming back to Barcelona. Also to provide me all what I needed down under, and specially, to organize such an emotive and awesome farewell BBQ in your house with all our team. Honestly, I reckon that night, we tasted wines that most of us we'll never see them again. Cheers!

Als membres del Servei de Microscòpia de la facultat (a l'**Anna, la Maria i l'Anna** "petita"). Gràcies per donar-me els coneixements necessaris de microscopia confocal, per passar hores barallant-nos amb les immunos del meu meravellós K_{ATP} (sobretot SUR1), i assegurar-nos que la colocalització és específica. Quin mal de cap tu!! . Ah, i també de que com processar després les imatges amb ImageJ.

A tots els membres que han format part o que encara formen part de la Unitat de Bioquímica. Nois/es, aquesta tesis, sincerament no hagués estat possible sense cap de vosaltres, a cadascú li pertany un petit tros d'això. A en **Lluís**, per trobar-te aquella nit pel Raval i comentar-me on podria fer la tesis, al **Feliu** pels seus concerts i intentar introduir-me en la música "alternativa", a l'**Helena**… ja no hi ha viatjes de tren interminables amb la nostra xerrera de divendres fins a Calella-Lloret, snif snif. A **Rosario** por tener ese carácter tan especial que al principio crees que te odia, pero poco a poco te demuestra que sólo tienes que saber cómo ganártela para recibir esos abrazos de madre. A **Mario** por ese humor, y esos mails, que no hace falta mencionar aquí. A **Carmencita**, que decir… a parte de toda tu ayuda a nivel técnico, paciencia y risas, por ser tu, tan madre (me llevo más de una lección), estar tan viva, pero especialmente por esos ánimos y palabras tan tiernas cuando más los necesitas. Nunca olvidaré nuestras charlas al principio de estar en Finlandia, pero que por suerte para mi no tuvieron que dudar mucho. También a las chicas del equipo ACTIMEL, **Erola, Irene**, y las "mamasitas" **Ivonne** y **Dami**, siempre que necesitaba un respiro o un cambio de aires, sólo tenía que aparecer por vuestro laboratorio para llevarme esa bocanada de energía que necesitaba. Así como a **Marga** y su determinación en tomar decisiones de futuro. A mi **Anabéééé**, ya sabes cómo nos reímos, no pierdas ese humor y esas palabricas tan castizas, asi cómo tampoco esos puntos de frikismo tan "sexis", sin ti no hubiera descubierto… CELEBRITIES, ejjeje!!!! A **Jose**, per posar aquest toc d'ART en totes les activitats del lab, i també pel seu ajut i per la seva sabiduría sobre que m'ha permès realitzar el mini-projecte de PCR-Array. Al **Jou**, sincerament tota una referència personal i científica, i per la seva disponibilitat sempre per respondre els meus dubtes o als problemes amb la micròglia. També a tot el seu agradable equip, en **Marco**, acabamos en parelelo, ehhh, **Francesco**, 100% italianini, i la **Núria**, gràcies per ajudar-me a manipular la micròglia, i tot els suggeriments per afrontar la tesis i buscar postdoc, sempre has anat un pas per endavant de mi, jeje. Y sobre todo al Dr. Antonio Valiente ;) es decir, **Tony**, el artista del lab, no hace falta que te agradezca todo tu apoyo, paciencia y tus ganas de hacer ciencia compartiendo tus conocimientos (sin mencionar reactivos, Ab's, etc). Me has ayudado tanto a nivel técnico… eres un crack!!! Además, siempre disfruto con tus interesantes puntos de vista u opiniones sobre temas que a mi se me escapan.

Aquí tenen especial importancia **TOTS els Neuroquímics**, per que gràcies a vosaltres aquests anys han estat una gran experiencia, no diré de color de violes, però inolblidable. Gracies per les hores passades junts al laboratori, m'emporto tots els nostres "gags personalitzats", els balls, cançons, tot el vostre recolzament (no

només científic), les tardes de birres, així com les activitats extra-laborals (teatres, concerts, etc). Un a un, a la **Neus** l'escaladora-patinadora (vamos, Barbie deportes de aventura) i el seu **Collins**, estic segur que ens continuarem veient durant molts anys, ànims que la tesis ja és teva; a l'espitosa **Montse**, vine a visitar-nos més sovint, se't troba a faltar…queda pendent la patinada, ah!! quan tu vulguis, ja saps on soc; al **Chiwi**, el bufón y el personaje más polivalente del laboratorio, ah! y también el segundo autor de mi primer paper… espero que hayan más. Tío, me perdí el TFC, pero espero no perderme la defensa de tesis… no crezcas nunca crack!; a la **Maggie**, per portar el color rosa al lab, i demostrar que mai es passa de moda; a l'**Alan**, per tenir converses tan transcendentals; a **Ivan**, curiosamente el físico en un master de neurociencias, que hacías allí?!?! Jejeje. Me fascina esa visión tan "diferente" de la ciencia; and to **Ania**, I'm so grateful about sharing those scientific moments with you, I wish you the best with your new family ;)

A tots els membres de Neurotec, pels moments inicials de l'empresa dins del mateix espai, rient i aprenent. **Noe**, encara recordo de la cara que posaves quan em veies amb els ratolins i et de sobte apareixies a l'altre punta de la sala amb cara de "jo això no ho penso fer mai". A **Juan** per ajudar-me amb els maleits westerns de Kir i SUR y a **Pilar**, por esa precisión y metodología tan risueña. **Andrew Bradshaw,** Quinesiologa de profesión (¿alguien sabía que era eso antes de conocerla?), me enseñó que con coraje y esfuerzo, una persona, puede llegar a ser lo que desea. I LOVE PISCO SOUR!

A mis compañeros del Master a los que les tengo especial cariño, hay que decir que todos han acabado antes que yo, grrrrr. Al **Dr. Javier Selva** y la **Dra. Empar Crespo** con los que he podido compartir dudas existenciales de: No sé q quiero hacer con mi vida… What's next? ¿Nos va servir para algo este master? Seguro que no :P También a la **Dra. Myriam Solar** (Mimi para los amigos) y ese maravilloso y divertidísimo Fin de Año en Madrid con sus amigos de la infancia. Me enseñaste la noche Madrileña y a cambiar la rutina familiar de cada navidad. Señores, aunque la distancia y la ciencia nos separe, no dejemos que se acaben esos cafés/birras :P

De mis estadas en el extranjero: 1) a los locos estudiantes de **Erasmus** con los que me junté durante esas largas noches en el frío Kuopio. Fortunately, I met such a nice and interesting people from around the World in Finland, specially from Spain, Netherlands and Australia. Also I'd like to thank to **Anu** and **Nanna** for your technical expertise in animal surgery and behavioral tests.

2) About my Ozzie experience, to all my QBI team, to **Jana,** my dear boss ;), without you the lab and science wouldn't be that funny, to **Chanel,** you have such sweet heart, to **Boris,** one day I'll beat you in tennis, mate!, to **Sophie,** I love your French boulangerie**, to Estella,** go harder on roller derby and to **Danisha,** missing your Indian food. And, to **Hannah** and **Christopher**, to enlighten me with that splendorous country called Australia! It was thrilling! Love you guys!

Un lloc especial per als meus companys Biolegs **(Paula, Vanix, Prats i Jordi**), que amb els anys, i el pas de la tesis… la nostra amistad s'ha fet més forta. Girona m'enamora! I això és gràcies a vosaltres!

También quiero agradecer a mis compañeros de Bioquímica y que curiosamente muchos hemos coincidido en el mundo de la neurociencia (¿nos hicieron a caso un lavado de cerebro? jejeje). Especialmente a las que hoy día forman parte de mi vida: **Maria** la "Tica", gracias a ti descubrí esas becas que me permitieron ir a México y empezar mi carrera científica, además de… con la excusa de ir a visitarte descubrí esa maravillosa Costa Rica. Y como no podía dejarme a la **Dra. Irene Bolea**, "Grande Irene, Grande!" Compañera del largo viaje del doctorado, con todos sus momentos ON/OFF, y que ha sido una maestra sobre la actitud que hay que tener frente a la vida. I have no words!!

A mi los que formaron parte de mi experiencia científica Mexicana, y que gracias a los **Doctores Alfredo Corona** y **Lucina Bobadilla** empecé a encontrarle el gustillo a esto de la investigación. También a los miembros del lab (**Citlali, Chio, Ana, Cesar**, y mi prima mexicana **Lorena** Ortega), por darme vuestro calor y hacerme sentir como en casa aún estando en un lugar muy distinto. De esta experiencia me llevé grandes amigos mientras hacía mis primeros pinitos en la ciencia, a **George, Chloé** y **Sarah**, ya sabeis que mi casa es vuestra casa, así que cuando queráis… Y especialmente a **Alba** y **Chivis**, que por suerte, nuestra experiencia mexicana ha durado mucho más tiempo y nos la hemos traído a Barcelona, la cual, espero que perdure siempre :D

A mi grupo de amigos de Lloret, los que han sufrido el seguimiento de mis años de universidad y doctorado dando ánimos, mis idas y venidas del país, y que por cierto me llaman empollón y piensan que lo único que hago es matar ratas (**Carles, Estela, Omar, Marc**, etc…). Ellos han conseguido que desconecte los findes que vuelvo a casa y hacen que tema la noche del pueblo. También a **Marta** alias "muerteeee", **Judith** y **María** y esos grandes fines de semana de escapadas, ya sea de aventura, casas rurales, montañismo o de relax con paseadas y cafés interminables. De Lloret seguro que me dejo a gente, pero daros todos por agradecidos. Especial mención en este apartado para **Raxaa** y **Keely,** sin vosotras Lloret no seria el mismo, me habéis enseñado a disfrutar de mi maravilloso pueblo, tan añorado durante estos años de doctorado.

También durante estos años, por suerte he compartido el piso con gente maravillosa, **Helene, Miki** y **Marisol,** conseguisteis que muchas noches separara trabajo de vida personal, vosotros también habéis sufrido el proceso :P

Amanda, tu aquí tienes un gran lugar, gran sufridora de la recta final del doctorado… gracias por compartir charlas de ciencia a cualquier hora, dudas existenciales mil, pero siempre… con copa de vino en la mano ;)

A todos mis amigos en Barcelona de origenes varios, a vosotros os debo el ocio de estos años, cines, teatros, cafés, birras, salidas en patines en cualquier momento en el que brillaba el sol, playas y alguna fiesta de vez en cuando.

Y por último a todos los miembros de mi maravillosa familia, vosotros sois los grandes impulsores de mi carrera, animando y apoyando todas mis decisiones des del primer día, mostrando entendimiento, amor incondicional y paciencia infinita, sobretodo en los momentos más difíciles. A mi hermano **Loren**, tu determinación a seguir con el negocio familiar me ha permitido llegar a ser lo que soy. Eres todo un ejemplo. **Mami**, cuántas veces hemos hablado de qué quiero hacer con mi vida… Eres la gran escuchadora de mi vida. A ti **Papa**, espíritu que hoy vuela libre y que eras gran sabio de la vida, a ti especialmente por enseñarme más cosas de las que era consciente, y especialmente por luchar y trabajar con la mama lo que hiciera falta para darme todo aquello que tu no pudiste tener.

También a mis abuelos, especialmente a mi nonagenario Yayo **Teodoro**, por esas clases de naturaleza con mi hermano durante los veranos de infancia, a mis tíos, primos y primitos, a todos os quiero…

A todos vosotros que de una u otra manera habéis tenido
que ver con en el proceso de elaboración de esta tesis…

INDEX

ABBREVIATIONS

ATP	adenosine triphosphate
BBB	blood brain barrier
bFGF	basic fibroblast growth factor
BrdU	bromodeoxyuridine
BSA	bovine serum albumin
CB	calbindin
CBA	cytometric bead array
CD11b	cluster of differentiation molecule 11b
CD3	cluster of differentiation 3
CNS	central nervous system
Csf1r	colony-stimulating factor 1 receptor
DIV	days in vitro
DMSO	dimethyl sulfoxide
DNA	desoxiribonucleic acid
Dz	diazoxide
EGF	epidermal growth factor
eGFP	enhanced green fluorescent protein
FACS	flow cytometry cell sorting
FJB	fluorojade B
Gbc	glibenclamide
GFAP	glial fibrilar acidic protein
H&E	haematoxylin-Eosin
IB4	isolectin B4
Iba1	ionized calcium binding adaptor molecule 1
IFNγ	interferon gamma
IL-10	interleukin-10
IL12p70	interleukin-12 p70
IL-1β	interleukin-1 beta
IL-6	interleukin-6

iNOS	inducible nitric oxide synthase
K_{ATP}	ATP-sensitive potassium channel
KCB	K_{ATP} channel blocker
KCl	potassium chloride
KCO	K_{ATP} channel opener
Kir	potassium inwardly rectifying channel
Kir6.1	potassium inwardly rectifying channel 6.1
Kir6.2	potassium inwardly rectifying channel 6.2
LPS	lipopolysaccharide
MCAO	middle cerebral artery occlusion
MCP-1	monocyte chemoattractant protein 1
MHCII	major histocompatibility class II
MMP	matrix metalloinpotease
MRI	magnetic resonance imaging
mRNA	messenger ribonucleic acid
$NC_{Ca\text{-}ATP}$	non-selective cationic channel
NeuN	neuronal specific nuclear protein
NGS	normal goat serum
NO	nitric oxide
NP	neural precursor
NRS	normal rabbit serum
NSC	neural stem cell
PB	phosphate buffer
PBS	phosphate buffer saline
PCR	polymerase chain reaction
PMN	polymorphonuclear neutrophils
PV	parvalbumin
RECA-1	rat endothelial cell antigen-1
ROS	reactive oxygen species
rt-PA	recombinant tissue plasminogen activator
S100β	*beta* subunit of the *S100* protein

SGZ	subgranular zone
SUR	sulfonylurea receptor
SUR1	sulfonylurea receptor isoform 1
SUR2A	sulfonylurea receptor isoform 2A
SUR2B	sulfonylurea receptor isoform 2B
SVZ	subventricular zone
TH	tyrosine hidroxylase
tMCAO	transient middle cerebral artery occlusion
TNFR1	receptor 1 of the tumour necrosis factor alpha
TNFR2	receptor 2 of the tumour necrosis factor alpha
TNFα	tumour necrosis factor alpha

SUMMARY

Stroke causes CNS injury associated with strong fast microglial activation as part of the inflammatory response. Fast activation of microglia in response to neuronal damage requires the rapid availability of a large amount of energy to trigger diverse cytotoxic or neuroprotective signals. ATP-dependent potassium (K_{ATP}) channels play important roles in many cellular functions by coupling cell metabolism to electrical activity. K_{ATP} channels were first detected in cardiac myocytes and later found in β-cells of the pancreas, skeletal muscle, neurons, smooth muscle, heart, pituitary, and tubular cells of the kidney. Our group and others have also demonstrated its expression in reactive microglia after brain injury.

In rat models of stroke, blockade of the sulfonylurea receptor (SUR), with glibenclamide (Gbc) reduced cerebral edema and infarct volume. Furthermore, clinical data suggest the effectiveness of Gbc to treat stroke. Gbc close the K_{ATP} channel by interaction with two drug-binding sites on SUR subunits, as well as, the astroglial $NC_{Ca\text{-}ATP}$ channel, which mediates the Gbc-induced prevention of edema after cerebral ischemia. In these studies however, the function of the K_{ATP} channel remained unclear. Therefore, as Gbc may bind to constitute functional K_{ATP} channels after ischemic stroke, other possible effects of Gbc might explain the effectiveness of this drug in the treatment of stroke. Giving the fact that, SUR1-regulated channels are exquisitely sensitive to changes in the metabolic state of the cell, and that microglia are sensing the environment, the expression of K_{ATP} channels in activated microglia, will couple cell energy to membrane potential. We herein postulate, that the effectiveness of Gbc to treat stoke, at least in part, is caused by the K_{ATP} channel closure expressed by activated microglia, which may then be critical in determining, their participation in the pathogenic process. Given the analogy with β-cells, K_{ATP} channel blockade in microglia would response faster and more efficiently to the external signals released after brain injury. If true, blockade of microglial K_{ATP} channel with low doses of Gbc during the early stages of stroke might foster neuroprotective microglial activity, could enhance ischemia-induced neurogenesis in the SVZ, and consequently will lead to an improved functional outcome.

The work presented in this thesis demonstrates that, Gbc improves functional neurological outcome in stroke, accompanied by neuron preservation in the core of the ischemic brain. In this region, reactive microglia from tMCAO rats upregulate the K_{ATP} channel, which makes microglia a target to Gbc actions in the early stages of stroke. Furthermore, Gbc also strengthens the neuroprotective role of microglia in the acute phase after focal cerebral ischemia, enhance long-term neurogenesis and brain repair processes. As such, identify microglial K_{ATP} channels as a key target for stroke treatment.

Overall, these results provide new therapeutic avenues for the treatment of other neurological disorders that involve microglia.

RESUM

Introducció - Els infarts cerebrals causen dany al SNC associat amb una ràpida activació microglial com a part d'una resposta inflamatòria. La ràpida activació microglial com a conseqüència al dany neuronal requereix d'una ràpida quantitat d'energia disponible per activar els senyals tan neuroprotectors com citotòxics. El canal de potassi depenent d'ATP (K_{ATP}) tenen un paper important en molts processos cel·lulars, els quals acoblen el metabolisme a l'activitat elèctrica cel·lular. Els canals K_{ATP} van ser primerament descrits en miòcits cardíacs, i seguidament en les cèl·lules beta del pàncrees, el múscul esquelètic i llis, neurones, cor, glàndula pituïtària i en les cèl·lules tubulars del ronyó. A més a més, el nostre grup amb altres han demostrat també la seva expressió en cèl·lules micròglials en resposta al dany cerebral.

En models d'isquèmia cerebral en rates, el bloqueig de la subunitat de sulfonilureas (SUR) amb glibenclamida (Gbc), redueix l'edema cerebral i el volum de l'infart. A més, resultats en estudis clínics suggereix la Gbc com a una fàrmac eficient per tractar els infarts cerebrals. La Gbc tanca el canal K_{ATP} a través de la interacció amb docs llocs d'unió a la subunitat SUR, així com, també causa el tancament del canal astroglial $NC_{Ca\text{-}ATP}$, el qual evita l'edema associat a la isquèmia. Tot i així, en aquests estudis, el paper del canal K_{ATP} segueix sense determinar. Per tant, com que la Gbc potencialment s'unirà també als canals K_{ATP} expressats per la micròglia, això donarà lloc a altres mecanismes per explicar l'efecte de la Gbc per tractar els infarts cerebrals. En aquest sentit, i degut a que els canals regulats per subunitats SUR1 són altament sensibles a canvis en el metabolisme cel·lular, i que la micròglia està contínuament percibint el seu entorn, l'expressió de canals K_{ATP} microglials, acoplaràn l'estat metabòlic de les cèl·lules amb el seu potencial de membrana.

Hipòtesi - Així doncs, postulem que l'eficiència de la Gbc per tractar els infarts cerebrals, al menys parcialment, és degut al tancament del canal K_{ATP} microglial, el qual serà crític en determinar la seva participació el procés patogènic. Donada l'analogia de que les cèl·lules beta pancreàtiques, el bloqueig del canal K_{ATP} microglial permetrà a la cèl·lula respondre més ràpidament i més eficientment als senyals externs alliberats al medi després del dany cerebral. El bloqueig del canal K_{ATP} microglial amb dosis baixes de Gbc durant les etapes primerenques de

l'isquèmia cerebral, promourà doncs la resposta microglial neuroprotectora, i potenciarà la neurogenesis de la SVZ derivada del dany isquèmic, donant lloc a una millora funcional.

Objectius – Els principals objectius d'aquesta tesi varen ser la caracterització de l'expressió dels diferents components del canal K_{ATP} *in vitro* i estudiar l'efecte de la Gbc en el procés d'activació de la línia cel·lular microglial BV2. Per altra banda, estudiar l'efecte de l'administració de dosis baixes de Gbc en un model d'isquèmia cerebral fent un estudi nivell histològic. En aquest apartat es posarà especial emfasis en els mecanismes de neuroprotecció, neurogenesis i de reparació cerebral en resposta al dany. Per acabar veure com això correlaciona amb millores funcionals i cognitives dels animals isquèmics.

Material i Mètodes – En un primer apartat es va realitzar la caracterització del canal K_{ATP} *in vitro* i es va estudiar l'efecte de la Gbc en el process d'activació de la línea cel·lular microglial BV2. En una segona fase, el model *in vivo* de treball va ser el de l'oclusió transitòria de l'artèria cerebal mitja (tMCAO) en rata. Els experiments es varen realitzar en mascles adults Wistar (250-300g) amb una oclusió de 60 o 90 min i amb o sense tractament amb Gbc (n=15-20/grup). Es valorà l'evolució clínica de cada rata amb tests neurològics y es va caracteritxar histologicament la lesió a curt termini (3 dies) i a llarg termini (1 mes) després de l'oclusió. En l'última fase es va utilitzar el model *in vitro* de neurosferes per estudiar la modulació de la neurogènesi per part del canal K_{ATP} microglial.

Resultats - Els resultats presentats en aquesta tesis demostren que, les cèl·lules microglials BV2 sobre-expressen el canal K_{ATP} en front d'un estímul pro-inflamatori *in vitro* i que la Gbc és capaç de modificar la seva activitat fagocítica, així com la secreció d'interleuquines. Per altra banda, el tractament de les rates isquèmiques amb Gbc augmenta la seva recuperació motora i cognitiva com a conseqüència d'una preservació neuronal en el nucli isquèmic tan a curt com a llarg termini. En aquesta regió, les cèl·lules microglials reactives de les rates tMCAO també sobre-expressen el canal K_{ATP}, convertint a la micròglia en una diana terapèutica per els efectes derivats de l'administració de Gbc en les etapes primerenques de l'infart cerebral. A més, la Gbc també fomenta el paper neuroprotector de la micròglia en l'etapa aguda de l'isquèmia cerebral, potencia la neurogènesi i els mecanismes de reparació del dany

cerebral a llarg termini, com per exemple la formació de nous vassos, tot això facilitant la millora neurològica dels animals. Per últim, amb l'assaig *in vitro* de neurosferes varem poder determinar com la potenciació de la neurogenesis observat *in vivo* era degut al bloqueig específic del canal K_{ATP} microglial. En aquest cas, la presencia de la Gbc estímula la secreció de factors solubles responsables de l'activació i migració de precursors neuronals, entre ells, el MCP-1.

Conclusions - Per tant, s'identifiquen els canals K_{ATP} microglials com a dianes terapèutiques per al tractament per l'isquèmia cerebral, el qual és capaç de promoure mecanismes de neuroprotecció, així com, potenciació de la neurogenesis i de les estratègies de reparació en resposta al dany cerebral.

En conjunt, tots els resultats d'aquesta tesis demostren que existeix una nova diana terapèutica amb la possibilitat de tractar altres alteracions neurològiques on la micròglia tingui un paper important.

Chapter 1.
INTRODUCTION

1.1 CNS DAMAGE AND NEURODEGENERATION: a challenge of the 21st century

The incidence of neurodegenerative diseases has increased in the global population and is likely to be the result of extended life expectancy brought about by better health care. Despite this increase in the incidence, there has been little improvement in the introduction of new disease-modifying therapies to prevent or delay the onset of these disorders, or reverse the degenerative processes in the brain. Neurodegenerative diseases include those of a chronic nature, e.g. Alzheimer's disease, Parkinson's disease, Huntington's disease and Amyotrophic Lateral Sclerosis as well as those originating from an acute initial insult such as traumatic brain injury and stroke. The major basic processes involved in neurodegenerative diseases of a chronic nature are multifactorial and caused by genetic, environmental and endogenous factors. Pathologically, these disorders share a common feature: the selective loss of a particular subset of neurons for as yet unknown reasons. Some general pathways might be recognized in different pathogenic cascades. They include protein misfolding and aggregation, oxidative stress and free radical formation, metal dyshomeostasis, mitochondrial dysfunction and phosphorylation impairment (Jellinger and Attems 2003) (**Fig. 1.1**).

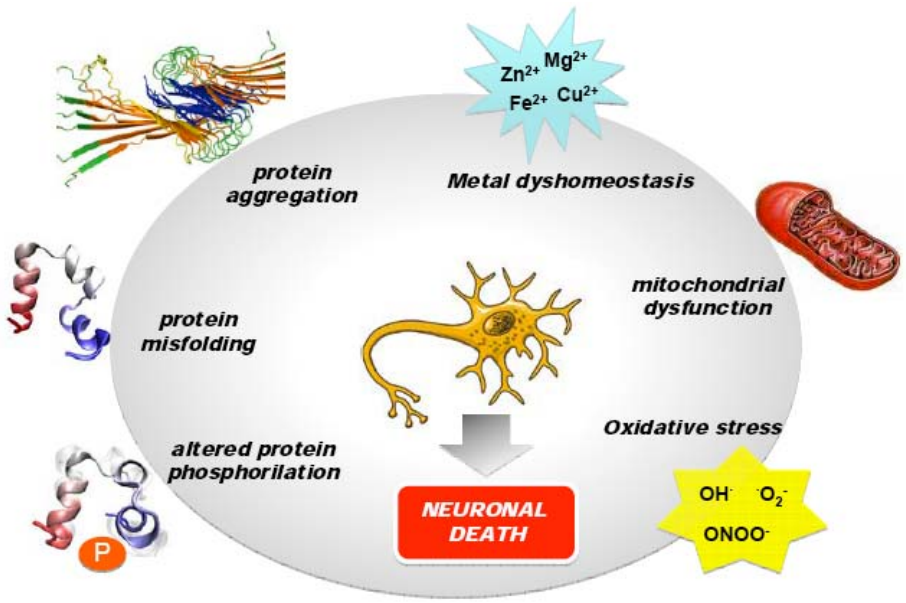

Fig. 1.1. Schematic pathways of the multifactorial events leading to neuronal death in neurodegenerative diseases. Modified from (Cavalli et al., 2008)

These events are probably responsible for calcium dysregulation and membrane depolarization that has also been identified as further common features of most neurodegenerative disorders (Skaper 2007). The most striking evidence pointing out the complexity of these neurodegenerative diseases is that to date any drug can either prevent the neurodegenerative process or restore the neurons that have died.

Pharmaceutical research has only been able to develop drugs that, at best, slightly modulate the symptoms in patients suffering from these disorders and improve their outcome.

1.2 STROKE

A stroke occurs when blood flow is interrupted or severely reduced to part of the brain. This depletion of blood to the brain deprives the tissue of essential oxygen, nutrients and to remove waste products, therefore brain cells quickly begin to die. Depending on the brain region affected, a stroke may cause paralysis, speech impairment, loss of memory and reasoning ability, coma, or death.

1.2.1 Historical perspectives and economical burden

In 1931, stroke was the second leading cause of death, after heart disease in the United States (US). Over the next 20 years, stroke death rates declined slightly, with crossover in 1937, but these 2 remained a close and essentially stable great decline in age-adjusted stroke death rates began, dropping modestly but steadily through the 1960s.

By 2008, the stroke mortality rate was three fourths less than its historic 1931 to 1960 norm. Cardiac mortality rates exhibited a similar pattern, suggesting parallel sources of change in death rates for the 2 major vascular diseases. After cardiovascular disease and cancer, stroke ranks as third cause of death in industrialized countries (**Fig. 1.2**)

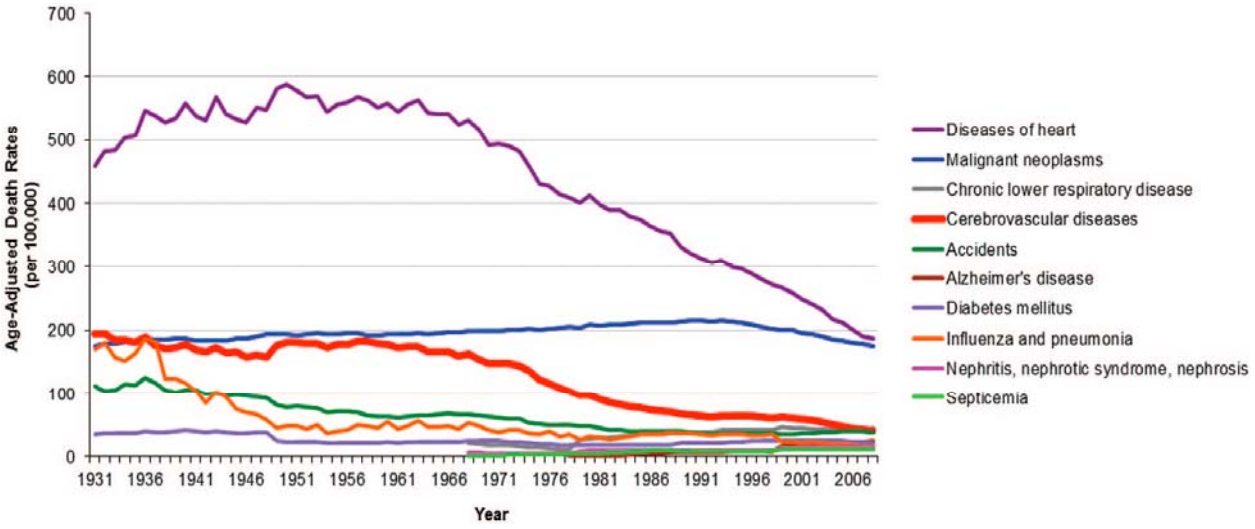

Fig. 1.2. Temporal trends in age-adjusted death rates for the top 10 causes of death in the United States from 1931 to 2008 (Towfighi and Saver 2011).

Declines in stroke incidence parallel the improvements in control of vascular risk factors. Consecutive National Health and Nutrition Examination Surveys reveal that treatment and control rates of hypertension have improved in the last decades. In addition, statin use has increased considerably in the US and studies revealed that simultaneously: (1) blood pressure decreased and awareness, treatment, and control of hypertension increased; (2) total cholesterol levels decreased and awareness, treatment, and control of hypercholesterolemia increased; and (3) smoking rates decreased (Towfighi and Saver 2011). Furthermore, improved acute stroke management has likely also contributed to the mortality decline, albeit to a lesser degree. Despite all these advances, stroke remains a leading cause of serious, long-term disability in the US, costing an estimated $73.7 billion in economic costs in 2010 and a human cost to patients and families that is incalculable.

As more and more individuals survive their strokes, the burden of poststroke disability will be an increasing public health priority (Paul et al., 2007), and burden varies greatly among countries, but low-income countries are the most affected (Johnston et al., 2009). Nonetheless, stroke remains the second leading cause of death worldwide, where over two thirds of stroke deaths worldwide occur in developing countries (Feigin 2005). Therefore, it will be of utmost importance to rigorously assess and design interventions to improve functional outcomes and quality of life after stroke.

1.2.2 Types of Stroke and main features

The most common type — ischemic stroke — results from blockage in an artery. The other type — hemorrhagic stroke — occurs when a blood vessel leaks or bursts (Amarenco et al., 2009; Grysiewicz et al., 2008).

A) Hemorrhagic strokes (13% of all cases)

Hemorrhagic stroke occurs when a blood vessel in your brain leaks or ruptures (**Fig. 1.3A**). Brain hemorrhages can result from a number of conditions that affect your blood vessels, including uncontrolled high blood pressure (hypertension) and weak spots in your blood vessel walls (aneurysms). A less common cause of hemorrhage is the rupture of an arteriovenous malformation — an abnormal tangle of thin-walled blood vessels, present at birth. There are two types of hemorrhagic stroke:

- Intracerebral hemorrhage**.** In this type of stroke, a blood vessel in the brain bursts and spills into the surrounding brain tissue, damaging cells. Brain cells beyond the leak are deprived of blood and are also damaged.
- Subarachnoid hemorrhage. In this type of stroke, bleeding starts in an artery on or near the surface of the brain and spills into the space between the surface of the brain and the skull. This bleeding is often signaled by a severe headache.

B) Ischemic strokes (87% of all cases)

Ischemic strokes occur as a result of an obstruction within a blood vessel supplying blood to the brain. The underlying condition for this type of obstruction is the development of fatty deposits lining the vessel walls (atherosclerosis) (**Fig. 1.3B**)**.** The most common ischemic strokes are:

- Thrombotic stroke. This type of stroke occurs when a blood clot (thrombus) forms in one of the arteries that supply blood to your brain. A clot usually forms in areas damaged by atherosclerosis.

- Embolic stroke. An embolic stroke occurs when a blood clot or other debris forms in a blood vessel away from your brain, commonly in your heart, and ends up blocking narrower brain arteries.

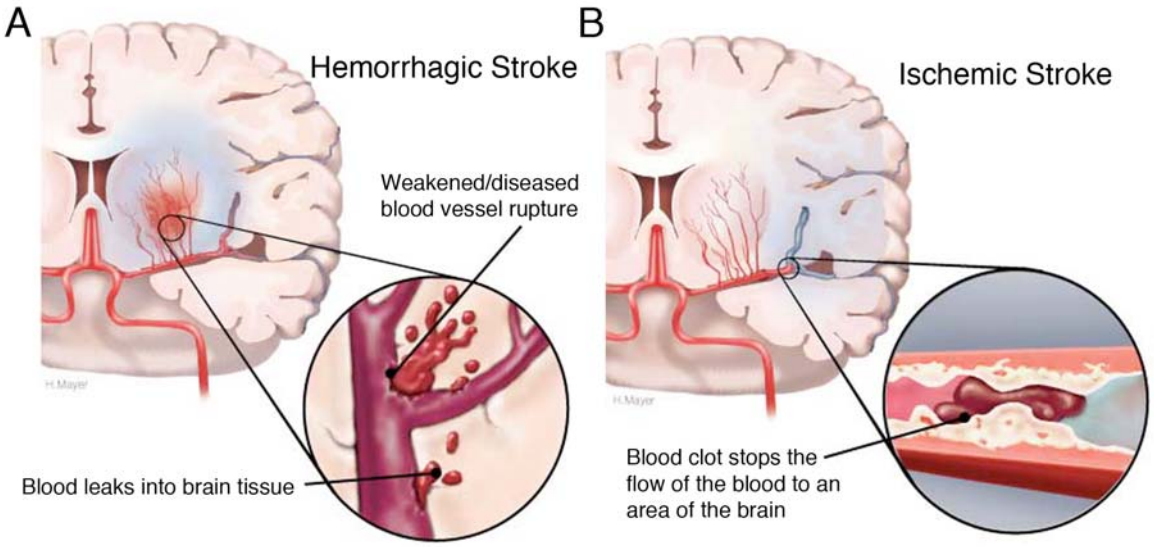

Fig. 1.3. Illustration of stroke subtypes. A) Hemorrhagic stroke. B) Ischemic stroke. Taken from the Heart and Stroke Foundation Canada (http://www.heartandstroke.com)

Although its origins can be different and the characteristics of a stroke will vary with each individual, there are a few classic signs that have been reported as being universal signals of a stroke.

- Walking problems.
- Trouble with speaking and understanding.
- Paralysis or numbness on one side of your body or face.
- Trouble with seeing in one or both eyes.
- Headache.

1.2.3 Risk Factors

Many factors can increase your risk of a stroke. A number of these factors can also increase your chances of having a heart attack (Gilman et al., 2005; Ingall 2004; Sahathevan et al., 2012). Stroke risk factors include: personal or family history of stroke, heart attack or transient ischemic attack; aging; High blood pressure; high cholesterol; smoking; diabetes, overweight; physical inactivity or cardiovascular

disease, including heart failure, a heart defect, heart infection, or abnormal heart rhythm.

In this line however, the diagnostic tools created with the arrival of computed tomography, magnetic resonance imaging (MRI), and other forms of vascular and cardiac imaging have improved the identification of risk factors for stroke according to its mechanism, hemorrhagic or ischemic, and according to the subtype of ischemic stroke (Bejot et al., 2007).

1.3 PATOPHYSIOLOGY OF STROKE

Ischemic stroke results from a transient or permanent reduction in cerebral blood flow that is restricted to the territory of a major brain artery. The reduction in flow is, in most cases, caused by the occlusion of a cerebral artery either by an embolus or by local thrombosis. In humans, ischemic stroke occurs most often in the area perfused by the middle cerebral artery (MCA) (Jin et al., 2010). Studies in animal models of stroke have provided an invaluable contribution to our current understanding of the pathophysiology of ischemic stroke. One of the most relevant stroke models involves transient or permanent middle cerebral artery occlusion (MCAO) in rats and mice (Jin et al., 2010; Lo 2008). Rats are one of the most suitable species for stroke study because of the pathogenetic similarities of strokes in rats and humans (Yamori et al., 1976) (**Fig. 1.4**).

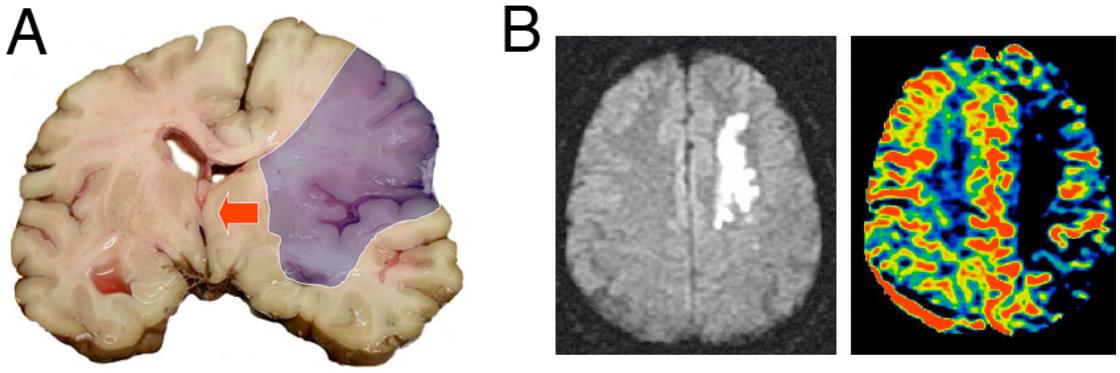

Fig. 1.4. Human MCA strokes. A) Photograph of acute MCA stroke. Schematic drawing depicting infarct area (blue shading) and midline shift, with a contralateral compression as a result of the edema were added (arrow). B) Magnetic resonance imaging in acute stroke. Diffusion-perfusion mismatch in acute ischemic stroke. The perfusion abnormality (right) is larger than the diffusion abnormality (left), indicating the ischemic penumbra, which is at risk of infarction.

1.3.1 Disruption of the neurovascular unit

Traditionally, the neuron is the key functioning unit in the brain. Thus, neurons have been considered the most important cell type within the central nervous system (CNS) and have been the focus of considerable brain pathology research. However, the brain is not made up of neurons only, but it also contains glial cells and cerebral endothelial cells. With a physical association in the same microenvironment, these cells interact with each other through various positive and negative feedback mechanisms. For instance, neurotransmitter release and reuptake at the synapse requires a signaling interaction between neurons and astrocytes (Hertz et al., 2007). In addition, the integrity of the blood–brain barrier (BBB) depends on the signaling between astrocytes and cerebral microvascular endothelial cells. Meanwhile, haemodynamic coupling between neuronal firing and vascular responses allows for matching of blood supply with metabolic demand (Chuquet et al., 2007). Therefore, stroke is neither a purely neuronal disease nor purely a blood disorder.

Protection of the neuronal microenvironment is provided by the neuron-glia-vascular unit, which includes endothelial cells, astrocytes, pericytes, neurons, and extracellular matrix around the vessels (Yang and Rosenberg 2011). Tight junction proteins form the first defense in the endothelial barrier disruption that leads to vasogenic edema and cell death. In stroke, the ischemic injury induces a molecular cascade that culminates in the formation of toxic proteases and free radicals, which contributes to tissue damage and the removal of dead cells. However, the same molecules that enhance damage in the early stages of the injury, perform essential functions in the recovery phase, drastically complicating the therapeutic use of these agents

In the acute phase (minutes to hours) of ischemic stroke, reactive oxygen species (ROS) and proinflammatory mediators (cytokines and chemokines) are released rapidly from injured tissue. These mediators induce the expression of the adhesion molecules on cerebral endothelial cells and on leukocytes and thus, promote the adhesion and transendothelial migration of circulating leukocytes (Jin et al., 2010). In the subacute phase (hours to days), infiltrating leukocytes release cytokines and chemokines, especially excessive production of ROS and induction/activation of

matrix metalloinproteases (mainly MMP-9), which amplify the brain-inflammatory responses further by causing more extensive activation of resident cells and infiltration of leukocytes, eventually leading to disruption of the BBB (Yang and Rosenberg 2011), brain edema, neuronal death, and hemorrhagic transformation (Amantea et al., 2009) (**Fig. 1.5**). However, many of these proinflammatory factors have a dual role at early and late stages of stroke.

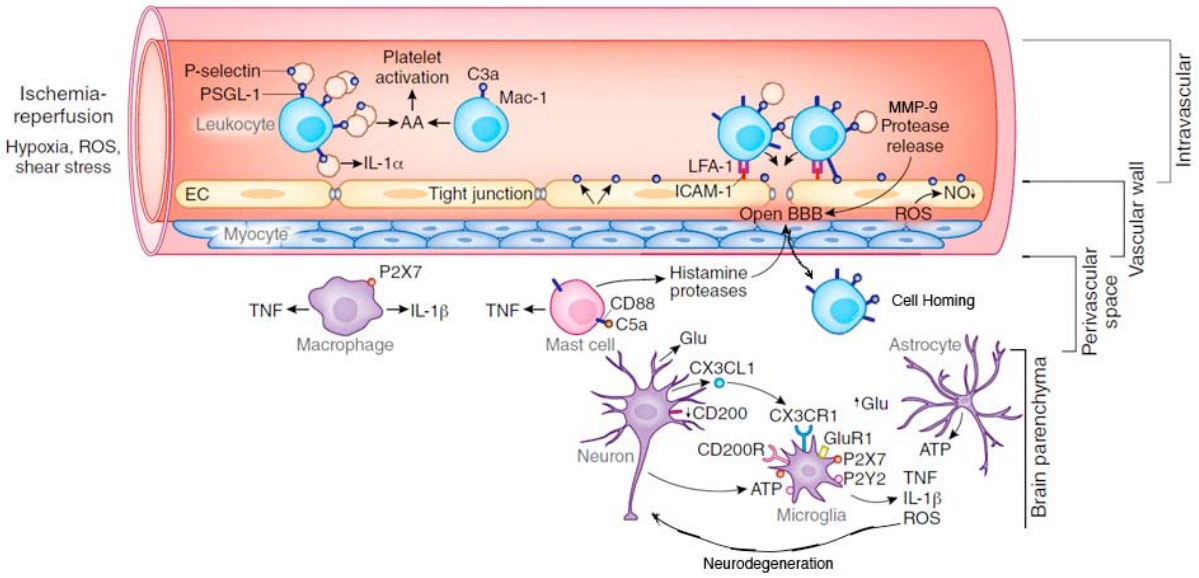

Fig. 1.5. Early vascular, perivascular and parenchymal events triggered by ischemia and reperfusion. Hypoxia, ROS and changes in shear stress initiate the cellular events induced by ischemia and reperfusion. MMP activation could lead to BBB breakdown and matrix proteolysis, facilitating leukocyte extravasation Cytokines (TNFα, IL-1β) are produced by mast cells and perivascular macrophages, providing further signals to guide leukocyte migration across the vessel wall. In the brain parenchyma, injured cells release purines (ATP), which act as early proinflammatory signals leading to production of cytokines and chemokines, leading to a neuronal damage. Adapted from Iadecola and Anrather 2011.

1.3.2 The penumbra or peri-infarct zone

With no doubt, the ischemic penumbra has emerged as a central concept in our current understanding of focal ischemic lesions of the brain. Named by analogy to the half-shaded zone surrounding a solar eclipse (Astrup et al., 1981), the penumbra lies just peripheral to the core zone of a focal ischemic lesion and can be defined as the viable tissue surrounding the irreversibly damaged ischemic core following cerebral ischemia (Ebinger et al., 2009). The initial phase of dysfunction is potentially reversible, prior to subsequent cell death. While some brain tissue may be irreversibly damaged, the other hypoperfused areas may be at risk but are

potentially salvageable. The degree of ischemia decreases with distance from the infarct core. The ischemic penumbra is a dynamic target that evolves over time and the infarct core evolves rapidly in the first few hours, therefore supporting the interventional concept that "time is brain" (Saver 2006). In early stages of large artery stroke most infarcts are surrounded by hypoperfused but still viable tissue. Both, the proportion of patients with an ischemic penumbra and the extent of the penumbra decrease with time from the symptom onset. The infarct core may grow into the penumbra or restored perfusion may prevent further infarct expansion (Ebinger et al., 2009) (**Fig. 1.6**).

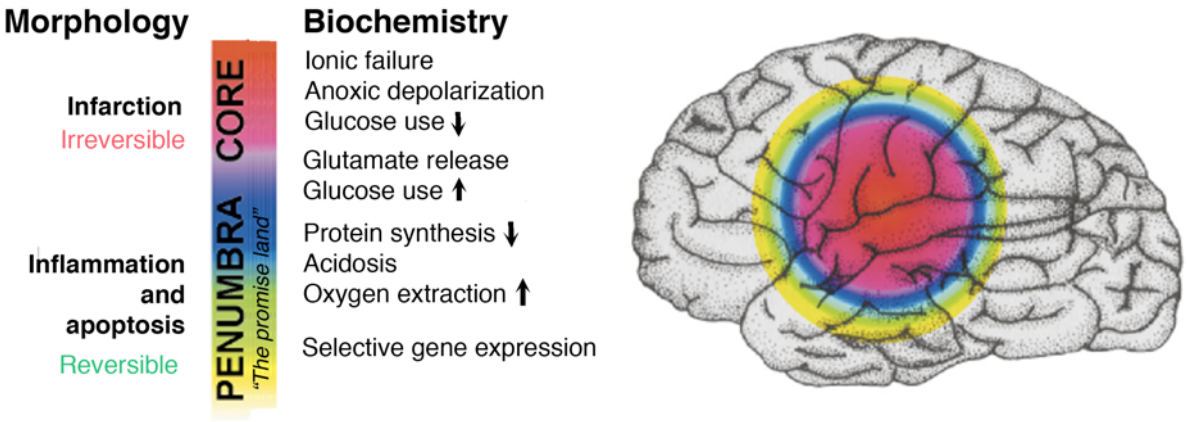

Fig. 1.6. The ischemic penumbra. A brain region of low perfusion in which cells have lost their membrane potential terminally ('core'), characterized mainly by necrotic death, is surrounded by an area in which intermediate perfusion prevails ('penumbra') and cells depolarize intermittently ('peri-infarct depolarization') which is a reversible event. Note that from the onset of the focal perfusion deficit, the core and penumbra are dynamic in space and time. Perfusion thresholds exist below which certain biochemical functions are impeded (color-coded scale). Adapted from Dirnagl et al., 1999.

If the central mechanism, which determinates the fate of cell in the penumbra, is its energy state(Liu and Levine 2008), several approaches being designed to improve it (Liu et al., 2010), and other molecular characteristics of the local injured tissue are under discussion. Even though the cellular and molecular changes characteristic for this area have been thoroughly studied in animal models in the last years, and the current therapies based on these searches proved to be unsuccessful (Arsene et al., 2011; Donnan 2008). Thus, the penumbra lies below the cerebral blood flow threshold for electrocortical silence but above that for massive ionic dyshomeostasis. The various attributes of the ischemic penumbra bear close scrutiny because they are

pivotal for grasping the essence of a focal ischemic lesion. They include the following (Dirnagl et al., 1999):

- The size of the early ischemic penumbra is substantial.
- The penumbra can be defined by its level of cerebral blood flow, above, approximately 20% to 40% of normal, and t is inherently unstable and at potential risk of irreversible deterioration.
- The penumbra is electrophysiologically dynamic in that it is the site of recurrent ischemic depolarization.
- The ischemic penumbra is thus metabolically unstable. Studies of neuron depolarization after MCA occlusion reveal approximately 50% reduction of cortical adenosine triphosphate (ATP) and phosphocreatine levels during reversible waves of depolarization, and complete depletion of these metabolites on terminal anoxic depolarization. Altogether indicate that:
- The ischemic penumbra is the site of severe metabolic stress.
- The lifespan of the penumbra is therefore limited.
- The therapeutic window for reperfusion in ischemic stroke is quite narrow.

1.3.3 Induced ischemic-damage timing

The development of tissue damage after an ischemic insult occurs over time, evolving within hours or several days and is dependent on both the intensity and the duration of the flow reduction, but also on flow independent mechanisms, especially in the peri-infarct brain regions (Hossmann 2006). A few minutes after the onset of ischemia, tissue damage occurs in the centre of ischemic injury, where cerebral blood flow is reduced by more than 80%. In this core region, cell death rapidly develops as a consequence of the acute energy failure and loss of ionic gradients associated with permanent and anoxic depolarization and release of excitatory amino acids, known as excitotoxicity (Dirnagl et al., 1999; Hossmann 2006; Mitsios et al., 2006). A few hours later, the infarct expands into the penumbra, an area of partially preserved energy metabolism, as a result of peri-infarct spreading depression and molecular injury pathways that are activated in the cellular and extracellular compartments. At this stage, cellular damage is mainly triggered by

excitotoxicity, mitochondrial disturbances, ROS production and programmed cell death (Lo et al., 2005; Mitsios et al., 2006). The evolution of tissue damage further perpetuates for days or even weeks as a result of secondary phenomena such as vasogenic edema and delayed inflammatory processes (Hossmann 1994) (**Fig. 1.7**).

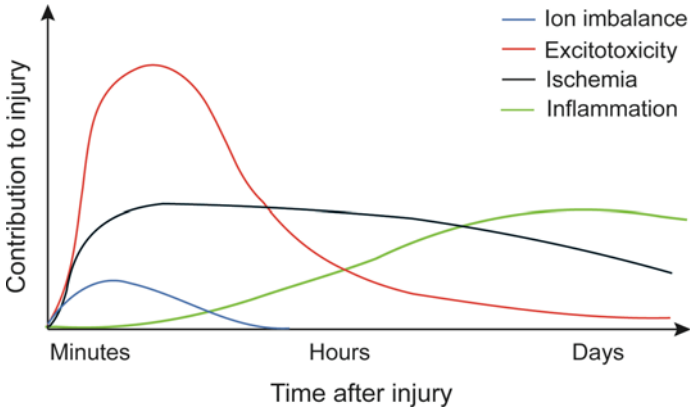

Fig. 1.7. Pathophysiology of traumatic brain injury and ischemia. The kinetics of the main events taking place in the lesioned CNS after an acute injury is shown. Taken from Ortega et al., 2012b.

There is increasing evidence demonstrating that neuroinflammatory processes play a pivotal role in the pathophysiology of brain ischemia. The inflammatory cascade is characterized by an immediate phase, which is initiated a few hours after stroke and may last for days and weeks as a delayed tissue reaction to injury (Dirnagl et al., 1999; Stoll et al., 1998). In addition to their deleterious contribution to ischemic tissue damage, inflammatory mediators may also exert beneficial effects on stroke recovery (del Zoppo et al., 2001; Denes et al., 2007; Kriz 2006). This point will be discussed in detail below.

1.3.4 Ischemic cascade

The brain is an organ that consumes much energy. This is partially due to the character of neurons; they possess excitable plasma membrane and a large amount of ATP is indispensable for maintaining ion gradient.

Acute brain damage can be viewed as an energy crisis that results from either an impaired energy production, as in ischemia or hypoglycemia, or pathologically elevated energy demands, as in a sustained seizure (Sapolsky 2001). During brain ischemia, the ionic gradients and membrane potential that power glutamate uptake are disrupted due to the oxygen deprivation and ATP deficiency, with extracellular

[Na^+] dropping, extracellular [K^+] rising and membrane potential dropping. The shift in ion gradients and loss of membrane potential cause the Na^+-dependent glutamate transporters to run backwards and release glutamate, inducing a rapid increase in extracellular glutamate levels. As glutamate is excitatory neurotransmitter acting through specific receptors expressed in neurons and glia, its accumulation outside the cell causes calcium ions to enter cells via NMDA receptor channels, leading to neuronal damage and eventual cell death, this event is called excitotoxicity. Moreover, glial cells, especially astrocytes, are the active players in ATP and glutamate signaling. ATP and glutamate coordinately activate astrocytes through the mobilization of internal Ca^{2+}, which, in turn, triggers the release of several neuroactive molecules from astrocytes, including ATP and glutamate. These 'gliotransmitters' signal either to astrocytes, where they generate Ca^{2+} waves, or to neurons, where they modulate synaptic transmission and neuronal excitability (Sun and Hu 2009).

Once neurons experience energy failure due to stroke, calcium accumulates in the intracellular space as a result of disturbed ion homeostasis explained above. This, in turn, activates many cellular processes, which culminate in cell death. In this cellular catastrophic cascade (**Fig. 1.8**), many organelles play important roles. In addition to the plasma membrane, cytosol is that first becomes exposed to the increased level of calcium. Many proteases, kinases and lipases are localized here, and are activated directly or indirectly by the ischemic insult. Some enzymes are pro-apoptotic ones, while others are anti-apoptotic. It is reported that neurons that would die later showed activated pro-apoptotic enzymes, but those that survive possessed activated anti-apoptotic molecules (Hayashi and Abe 2004).

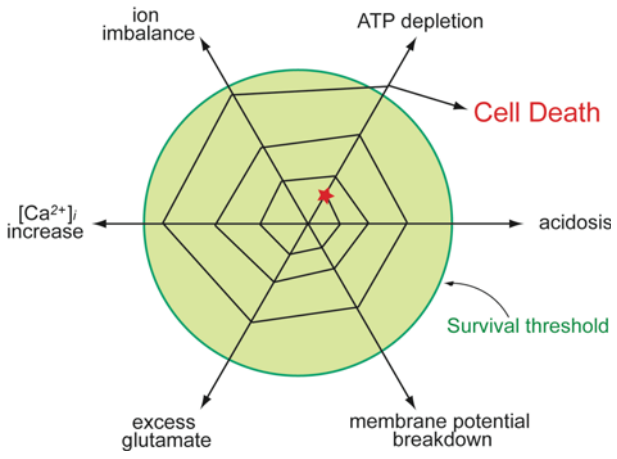

Fig. 1.8. Accelerating loops of excitotoxicity and cell death. An initial insult causes a limited disturbance of cellular homeostasis; the starting point (red star) being for example the ATP depletion due to a discrete localized hypoxia. Looping mechanisms cause an ever increasing mitochondrial dysfunction and acidosis, an increase in $[Ca^{2+}]_I$ and in glutamate release, with membrane depolarization and ion imbalance. Beyond a certain threshold, the activation of cell death program would further accelerate the cycles leading to neuronal death. Taken from Ortega et al., 2012b.

After stroke, collateral vessels maintain sufficient blood flow to allow the potential survival of cells in areas adjacent to the core of the infarct. Cells in this penumbra area have impaired function but remain viable for a period of time (Dirnagl et al., 1999). In the area where oxygen depletion is only moderate, cells can activate their own apoptotic program, which requires ATP to be executed. The mitochondria play a role in either necrotic or apoptotic cell death, depending on the severity of the initial insult (Halestrap 2006). Apoptosis is favored after mild insults when ATP production of the cell is relatively well preserved, whereas necrosis occurs in response to a severe insult, such as severe ischemia. Cells then die rapidly due to cell swelling, activation of proteases, and cell membrane breakdown. Thus, for each cell type, the factors that determine the pattern of cell death at any moment are the intensity of the lesion, the $[Ca^{2+}]_i$ and the cellular energy production. The cell then prevents the uncontrolled release of intracellular compounds (e.g. glutamate) and the subsequent inflammatory response of tissue. As ATP decreases, the necrotic process starts presenting a hybrid pattern involving both cell death types (**Fig. 1.9**).

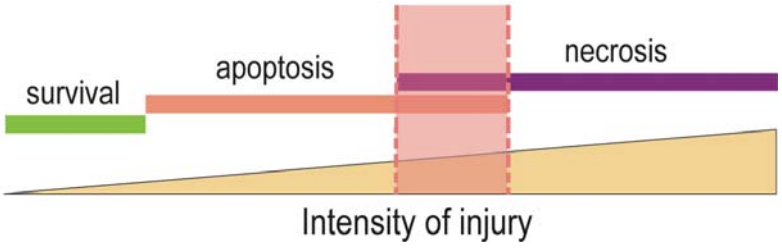

Fig. 1.9. Under mild injury, the initial aggression would be compensated by cellular defense mechanisms; with a more severe damage, neurons would die by apoptosis, necrosis or a mixed program. Taken from Ortega et al., 2012b.

Therefore, targeting a single point or a single pathway may not yield sufficient protection in stroke. Rather, the emphasis should be on the targets that mediate cross-talk between multiple cell death mechanisms (Sun and Hu 2009).

1.4 NEUROINFLAMMATION: FRIEND OR FOE?

Inflammatory cells participate in tissue remodeling after CNS injury. Microglia is considered the resident immune cells of the CNS and are normally the first cells in the brain to react to acute injury and recruit astrocytes.

1.4.1 Microglia in healthy brain

Resting microglia is extremely dynamic *in vivo*, perpetually changing their morphology by extending and retracting highly motile processes on a time scale of minutes and closely associated with both neurons and astrocytes (Davalos et al., 2005; Nimmerjahn et al., 2005). This unexpected finding led to a series of discoveries suggesting potential roles of microglia in postnatal development, adult neuronal plasticity, and circuit function. In normal conditions microglia normally monitor the brain environment and respond to the functional state of synapses by sensing and eliminating defunct synapses (Tremblay et al., 2011; Wake et al., 2009), controlling synaptogenesis (Bessis et al., 2006) and clearing newborn adult hippocampal neuroprogenitors (Sierra et al., 2010). All these results suggest that microglia is a highly motile cell, which facilitate its efficient immune surveillance of the brain (**Fig. 1.10**).

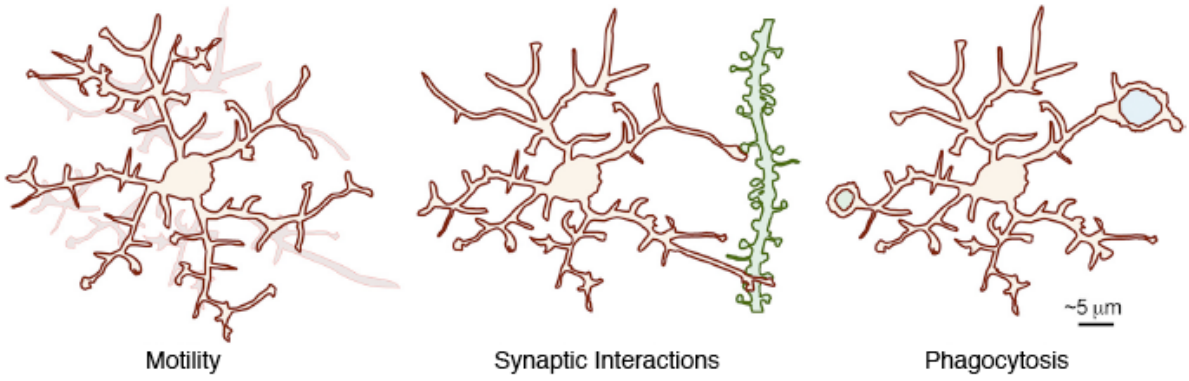

Fig. 1.10. Overview of microglial behavior in the healthy brain. Highly motile microglial processes continuously remodel their local environment (left), structurally and functionally interact with synaptic elements (middle; dendritic branch and spines, green) through direct contacts and exchanges of molecular signals, and contribute to restructuring of neuronal circuits by phagocytosing synaptic elements and newborn cells (right; cellular inclusions, blue and green). Taken from Sierra et al., 2010.

1.4.2 Cellular response to injury

Post-ischemic inflammation is characterized by a rapid activation of resident microglial cells and by infiltration of neutrophils and macrophages in the injured parenchyma, as demonstrated both in animal models (Schilling et al., 2003) and in stroke patients (Price et al., 2004). Within hours after the ischemic insult, increased levels of cytokines and chemokines enhance the expression of adhesion molecules,

such as intercellular adhesion molecule 1, on cerebral endothelial cells, facilitating the adhesion and transendothelial migration of circulating neutrophils and monocytes. These cells may accumulate in the capillaries, further impairing cerebral blood flow, or may migrate into the brain parenchyma where they release neurotoxic substances, including pro-inflammatory cytokines, chemokines and oxygen / nitrogen free radicals (Yang and Rosenberg 2011). Four to six hours after ischemia, astrocytes become hypertrophic, while microglial cells retract their processes and assume an amoeboid morphology that is typical of activated microglia. Twenty-four hours after MCA occlusion the microglial reaction is well developed in the ischemic brain, particularly in the penumbra (Dirnagl et al., 1999). Amoeboid microglia upregulate a variety of surface molecules and the release a wide panel of cytokines.

1.4.3 Enzymes

Infiltrating neutrophils, microglia / macrophages and endothelial cells may release toxic amounts of nitric oxide (NO) via the inducible nitric oxide synthase (iNOS) isoform, which is strongly induced following the ischemic insult (Iadecola 2011). Immediately after brain ischemia, NO produced by endothelial NOS exerts beneficial effects by promoting vasodilatation, whereas NO produced during later stages of injury by overactivation of neuronal NOS and de novo expression of iNOS contributes to ischemic tissue injury (Kettenmann et al., 2011; Mohammadi et al., 2011). Despite substantial evidence underlying the deleterious role of iNOS-derived NO in ischemic pathophysiology (Iadecola and Anrather 2011; Mohammadi et al., 2011; Moro et al., 2004), by using chimeric iNOS-deficient mice, a recent study has suggested that this enzyme may not be implicated in the development of brain damage induced by transient focal ischemia (Prüss et al., 2008), but further evidence is needed to confirm this hypothesis. Excessive production of NO by iNOS is responsible for cytotoxicity by inhibiting ATP-producing enzymes, by producing peroxynitrite and by stimulating other pro-inflammatory enzymes such as COX-2. Moreover, NO may promote ischemic cell death via S-nitrosylation and, thereby, activation of MMP-9 (Amantea et al., 2009).

1.4.4 Cytokines and Chemokines

After an ischemic insult, the expression of several cytokines is upregulated in cells of the immune system, but also in resident brain cells, including neurons and glia. While some cytokines, such as IL-1β, appear to exacerbate cerebral injury, others (e.g. IL-6, IL-10 and transforming growth factor-beta) seem to provide neuroprotection (Iadecola and Anrather 2011; Mabuchi et al., 2000). The main source of cytokines after cerebral ischemia are endothelial cells, microglia and macrophages, although it may also be expressed by neurons and astrocytes (Mabuchi et al., 2000). In addition to IL-1β, brain injury induced by focal ischemia is characterized by a significant and rapid upregulation of tumor necrosis alpha (TNFα), as demonstrated both in animal models and in stroke patients. For example, TNFα secretion is crucial for rapid autocrine microglial activation with both neuroprotective and cytotoxic effects, a process that is also fed by TNFα released by reactive astrocytes (Sriram and O'Callaghan 2007). The opposing TNFα actions depend on the activation of two specific receptors: TNFR1, which has a low affinity and an intracellular death domain, and TNFR2, which has a high affinity and is mainly involved in neuroprotection (Fontaine et al., 2002). Therefore, at low concentrations, TNFα only binds to TNFR2 and potentiates neuronal survival, whereas the subsequent TNFα secretion by microglia and astrocytes activates TNFR1 in neurons and astrocytes and contributes to cell injury (Bernardino et al., 2008). Thus, the roles of both receptors in modulating cell death / survival remain unclear, as both receptors may activate intracellular mechanisms contributing either to the induction of cell-death mechanisms or to antiinflammatory and anti-apoptotic functions (Hallenbeck 2002). Among other cytokines involved in stroke pathophysiology, IL-10 and transforming growth factor-beta have been demonstrated to have anti-inflammatory effects, providing significant protection against ischemic brain damage (Iadecola and Anrather 2011).

Chemokines are regulatory polypeptides that mediate cellular communication and leukocyte recruitment in inflammatory and immune responses. Increased mRNA expression for monocyte chemoattractant protein-1 (MCP-1) and macrophage inflammatory protein-1 alpha has been described in the rat brain after focal cerebral ischemia (Hinojosa et al., 2011; Jin et al., 2010; Liberto et al., 2004).

Expression of MCP-1 has been described in neurons 12 h after focal brain ischemia, but also in astrocytes and microglia at later stages following the insult. Moreover, MCP-1, as well as stromal cell-derived factor-1a, has been shown to trigger migration of newly formed neuroblasts from neurogenic regions to ischemic damaged areas (Amantea et al., 2009; Ekdahl et al., 2009; Mantovani et al., 2004). Another chemokine implicated in ischemic pathophysiology is fractalkine, whose expression is increased in neurons and in some endothelial cells after a focal ischemic insult. Interestingly, expression of its receptor, CX3CR1, was observed only in microglia / macrophages, suggesting that fractalkine is involved in neuron-microglia signaling (Mantovani et al., 2004; Tremblay et al., 2011).

1.4.5 Microglia, inflammation and neurotoxicity

All these findings suggest that microglia, when overactivated, serve to enhance and amplify neuronal damage induced by pathological stimuli and toxins. In turn, this activity likely induces more widespread damage to neighboring neurons (reactive microgliosis) (Acarin et al., 2000; Block et al., 2007). Taken together, these studies indicate that two types of signal can overactivate microglia: the direct stimulation of microglia by environmental toxins or endogenous proteins, and neuronal damage and consequent reactive microgliosis. Thus, microglial overactivation initiated by early immunological insult or direct injury to neurons might be propagated and potentially amplified throughout the course of neurodegenerative diseases, driving the continuous and cumulative loss of neurons over time. However, when the ability to activate protective mechanisms fails, or when they are overwhelmed by an excessive inflammatory response, microglia initiate neuronal death and drive the progressive nature of neurodegenerative disease (Block et al., 2007; Moss and Bates 2001; Sawada et al., 1989) (**Fig. 1.11**). Normally these kinds of events are done in chronic neuroinflammation diseased, such as Alzheimer's disease, Parkinson's disease, Huntington's disease, Multiple Sclerosis and Amyotrophic Lateral Sclerosis, resulting in a perpetuating cycle of neuron death.

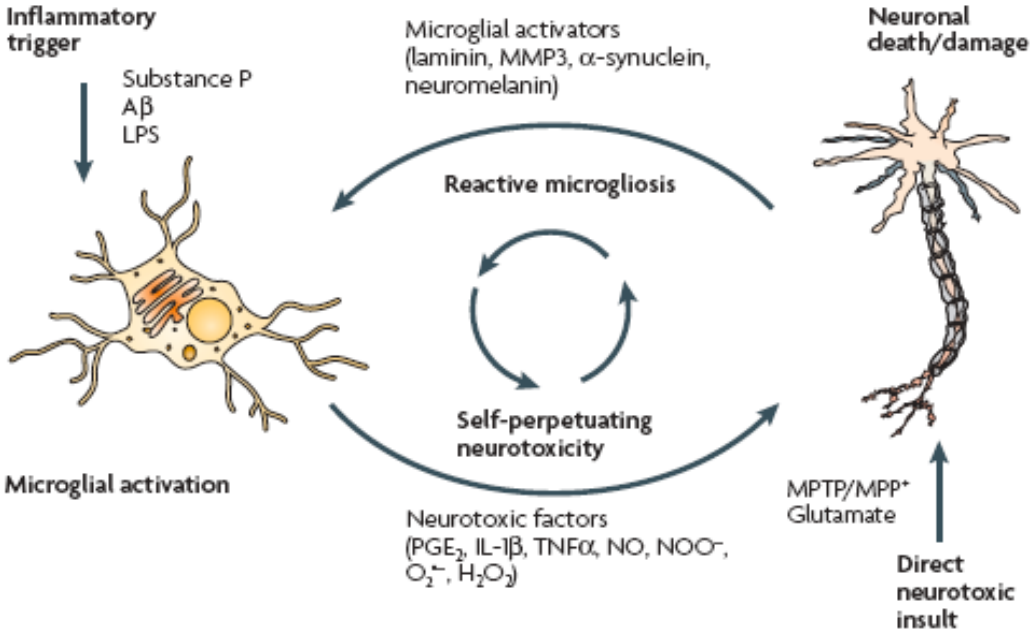

Fig. 1.11. Reactive microgliosis drives progressive neurotoxicity. Microglia can become overactivated and cause neurotoxicity through two mechanisms. 1) Microglia can initiate neuron damage by recognizing pro-inflammatory stimuli. 2) Microglia can become overactivated in response to neuronal damage (reactive microgliosis), which is then toxic to neighboring neurons, resulting in a perpetuating cycle of neuron death. Taken from Block et al., 2007.

Secondly, recent reports indicate that pattern recognition receptors (PRRs) are tools used by microglia to identify neurotoxic stimuli and that stimulation of NADPH oxidase activity is the predominant mechanism through which microglia produce neurotoxic ROS. Thus, the identification of these crucial participants in microglia-mediated neuronal injury provided the insight necessary for the development of novel markers that specifically define deleterious proinflammatory microglial activation, that already belong to the classically activated or M1 phenotype (**Fig. 1.12**). PRRs are generally constitutively expressed to identify and bind pathogen-associated molecular patterns (PAMPs), and are therefore crucial to the innate immune response. However, in the case of microglia-mediated neurotoxicity, receptors responsible for host defense and phagocytosis often mediate neuronal damage in the absence of a microbial pathogen, suggesting that non-pathogenic stimuli are misinterpreted with dire neurotoxic consequences (Block et al., 2007).

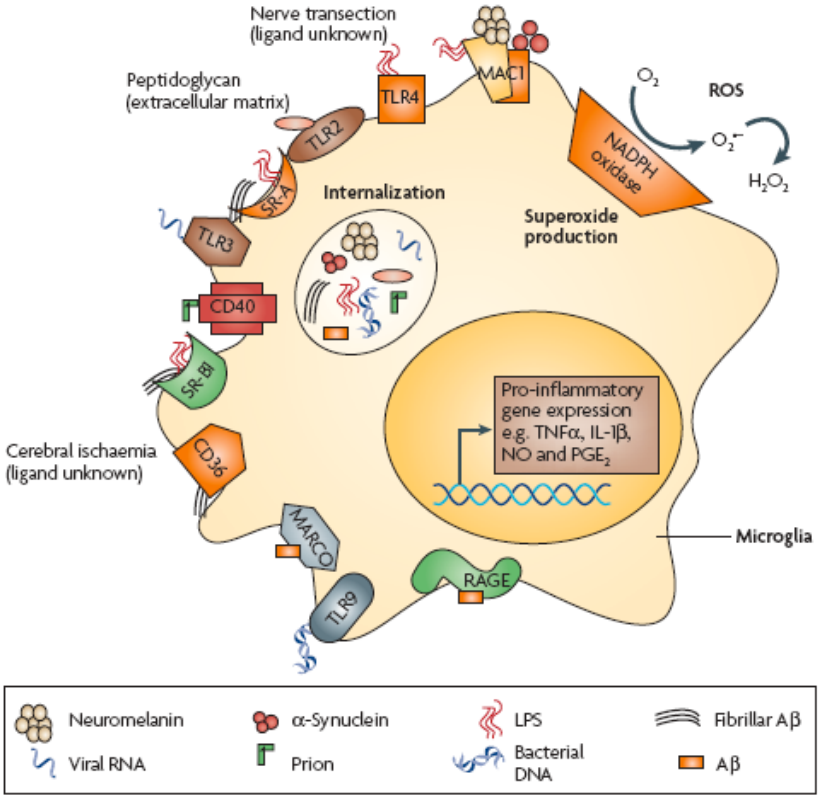

Fig. 1.12. Microglial PRRs identify neurotoxic and pro-inflammatory ligands. Microglia actively monitor the brain environment with pattern recognition receptors (PRRs). PRRs are responsible for several phagocyte functions such as the identification of pathogens, the production of extracellular superoxide, the release of pro-inflammatory compounds and the removal and destruction of toxic stimuli through internalization and phagocytosis. Taken from Block et al., 2007.

1.4.6 Neuroinflammation as a retaliatory mechanism against CNS damage

As described above a marked recruitment, proliferation and activation of microglial cell precursors from the blood can be detected in damaged regions of the brain (Soulet and Rivest 2008), and when the BBB integrity has been compromised by the insult, a variety of inflammatory cells, such as activated leukocytes, rapidly penetrate the brain (Frijns 2002). These inflammatory cells have a dual role in the early and late stages of stroke. For instance, regardless of the cellular origin, MMP-9 is initially detrimental but promotes brain regeneration and neurovascular remodeling in the later repair phase (Amantea et al., 2009), and therefore may be involved in further brain damage or repair. In addition to microglia, astrocytes and endothelial cells are also involved in the intracerebral immune response to CNS injury. All these cell types act, in part, by secreting cytokines, chemokines, neurotrophic or neurotoxic factors (Bailey et al., 2006). For example, activated

microglial cells migrate towards dying neurons in response to neuroinflammation and can exacerbate local cell damage (Acarin et al., 2000; Streit 2005). Microglia also respond to interferon gamma (IFNγ) and TNFα by expressing class I and II major histocompatibility complex molecules (MHC-I and -II, respectively) and co-stimulatory molecules, which allows microglia to function as antigen-presenting cells (Kettenmann et al., 2011). Astrocytes that also express MHC molecules, but lack co-stimulatory molecules, can present antigen to primed memory T cells but not to naive T cells (Molina-Holgado and Molina-Holgado 2010). Furthermore, astrocytes respond by releasing other complement proteins and acute-phase proteins, such as α1-antichymotrypsin and α2-macroglobulin, as well as neuronal growth factors and cytokines cells (Kettenmann et al., 2011). As a hallmark, microglia are normally the first cells in the brain to react to acute injury and recruit astrocytes by secreting acute-phase proteins, particularly those belonging to the complement system, and also by releasing cytokines, such as interleukin IL-1β and TNFα, and ROS species cells (Kettenmann et al., 2011). Unlike their role in phagocytosis, activated microglia are classified as antigen-presenting cells, as they upregulate MHC-II, and under certain conditions following brain inflammation or injury, activated microglia mediate neuronal damage and aid in brain repair, providing a potent neuroprotection (Carson et al., 2006; Kitamura et al., 2004; Lalancette-Hébert et al., 2007; Neumann et al., 2006; Shaked et al., 2005; Streit 2002) or acting as a proneurogenic influence that supports the different steps of neurogenesis (Ekdahl et al., 2009).

Microglia do not constitute a unique cell population, but rather, show a range of phenotypes (Schwartz et al., 2006) that are closely related to the evolution of the lesion process (Graeber and Streit 2010). In a dynamic equilibrium with the lesion microenvironment, these phenotypes range from the well-known proinflammatory activation state (classically activated or M1) to a neurotrophic one that is involved in cell repair and extracellular matrix remodeling (alternatively activated or M2) (Dirscherl et al., 2010). Thus, microglia differentiate into cells that exacerbate tissue injury or promote CNS repair when they receive signals from the close surroundings. M1 microglia/macrophages, activated via toll like receptors (TLRs) and IFNγ, produce proinflammatory cytokines and oxidative metabolites that

facilitate their role as indiscriminate killers of infectious agents and tumor cells (Mantovani et al., 2004), with collateral damage to healthy cells and tissue. Conversely, M2 microglia/macrophages form in the presence of IL-4 or IL-13, downregulate inflammation, and facilitate wound healing, with the induction of scavenger receptors and matrix-degrading enzymes that enhance phagocytosis and promote tissue repair, i.e., by promoting angiogenesis and matrix remodeling (Mantovani et al., 2004; Sica et al., 2006). Furthermore, the crosstalk between elements of the neuroinflammatory response and those that interact with neural stem cells might activate endogenous neurogenesis and facilitate brain repair (Rolls et al., 2007) (**Fig. 1.13**).

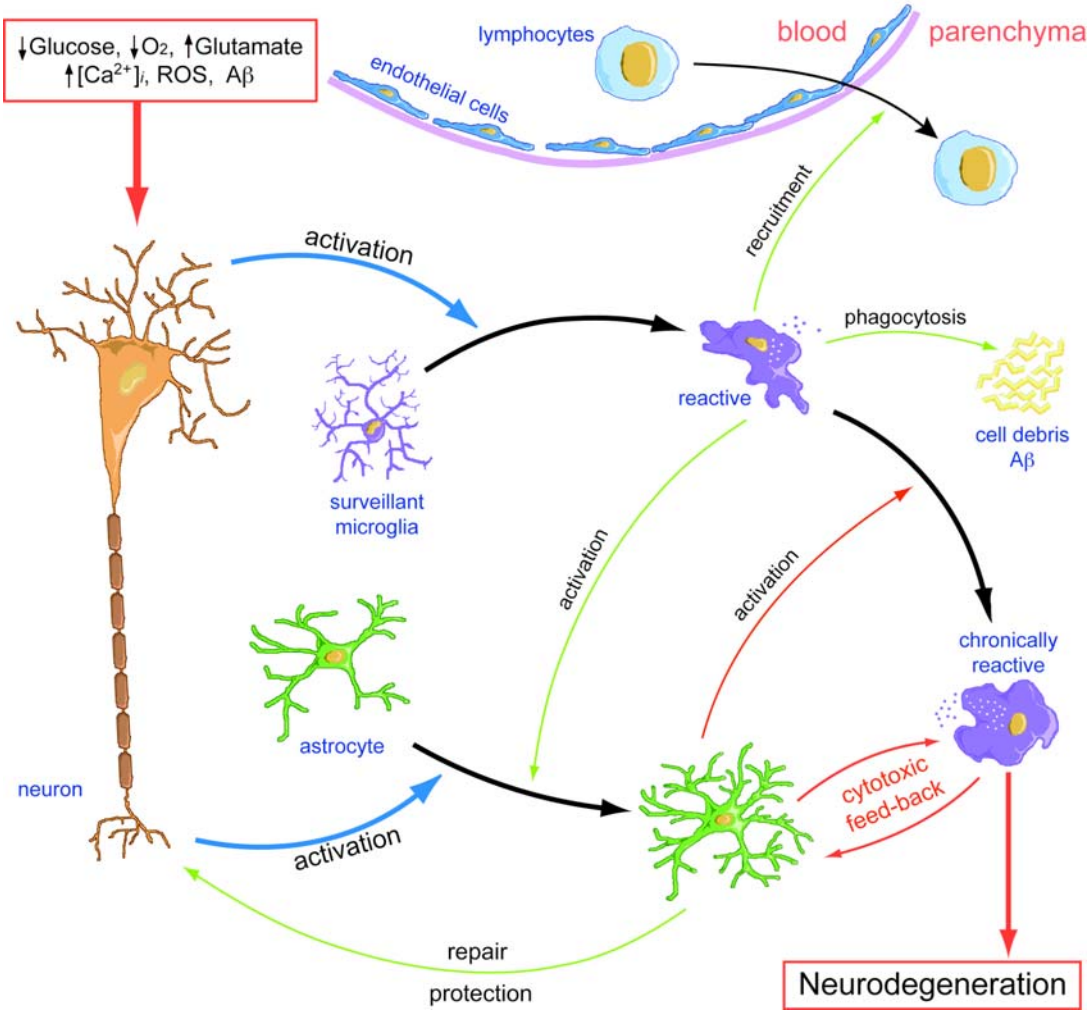

Fig. 1.13. Cellular processes involving neuroinflammation after brain injury. Physiological modifications (molecules inside a red square) affect neurons, and consequently the release of mediators causing astrogliosis and microgliosi. Reactive microglia mediate different pro-inflammatory and neuroprotective processes (green arrows) in coordination with reactive astrocytes. Overactivated microglia becomes dysfunctional and adopt a chronic reactive phenotype mostly cytotoxic that directly participates of neurodegeneration. Astrocytes contribute to this activity also by releasing activation signals (red arrows). Taken from Ortega et al., 2012b.

1.5 MICROGLIA AND NEUROGENESIS

In the adult brain two canonical neurogenic niches are known, the subgranular zone (SGZ) and the subventricular zone (SVZ), where form new dentate granule cells and olfactory bulb interneurons, respectively (**Fig. 1.14B, C**). Pathological conditions however, such as stroke or status epilecpticus influence neurogenesis, and can stimulate the formation of new neurons in SVZ and SGZ towards the lesion (Arvidsson et al., 2002; Arvidsson et al., 2001; Bengzon et al., 1997; Parent et al., 2002; Parent et al., 1997).

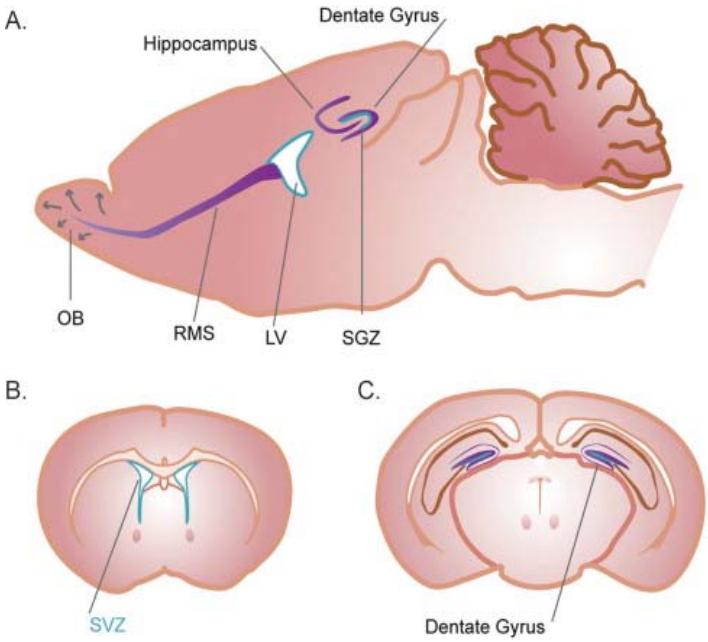

Fig. 1.14. Neurogenic niches of the adult rodent brain. Shown in a sagittal section (A) and in coronal sections (B and C): the subventricular zone (SVZ) that surrounds the lateral ventricle (LV) and the subgranular zone (SGZ) in dentate gyrus of the hippocampus. The neural stem cells in the SVZ proliferate locally to generate neuronal progenitors and neurons, which migrate along the rostral migratory stream (RMS) to reach the olfactory bulb (OB) and integrate into the existing circuitry to contribute towards the olfactory function. In the hippocampus, neural stem cells residing along the subgranular zone of the dentate gyrus continue to produce neurons that contribute towards hippocampal functions such as spatial learning and memory. Taken from Vukovic et al., 2011.

1.5.1 Adult neurogenesis

Adult neurogenesis is the production of new neurons into the adult brain. This is a multistep process involving proliferation of neural precursor cells (NPs), their differentiation into lineage-restricted immature neurons, and the progressive maturation of these newborn cells into a new functioning neuron. It's a process not an event. It involves decisions into the precursor cell level, such as whether symmetric division (with identical daughter cells), or asymmetric division (with two different daughter cells) occurs. After asymmetric division, various factors determine when the progeny is to become a neuron. Neurogenesis includes securing

the survival of the new cells, migration of the differentiating progeny and the differentiation process itself, it entails sending out the cellular processes and integrate properly into the synaptic network (Kempermann 2006). Neurons are originated from neural stem cells (NSC) throughout the entire lifespan, and might continuously replace dying neurons or contribute to specific brain functions and plasticity, for instance to replace continuously dying neurons in the olfactory bulb (Merkle et al., 2007; Toni et al., 2007; van Praag et al., 2002) (**Fig. 1.14A**).

1.5.2 Stroke-induced neurogenesis

The effects of ischemia and hypoxia have been studied primarily in the context of animal models of stroke. Ischemia, as explained above, causes a complex response that activates local precursor cells in the neurogenic. Cell proliferation in the SGZ is induced in many models of ischemic brain injury (Arvidsson et al., 2001; Jin et al., 2001; Liu et al., 2000). This effect occurs even in the absence of direct visible damage of the hippocampus, supporting the idea that not just gross local regulatory mechanisms apply. This activation of progenitors cells is NMDA-receptor activation-dependent (Arvidsson et al., 2001).

Although a number of studies have reported regenerative neurogenesis in non-neurogenic regions after ischemia (Arvidsson et al., 2002; Nakatomi et al., 2002; Parent et al., 2002), there is little doubt that ischemia and hypoxia can influence precursors cells and adult neurogenesis in neurogenic regions (Arvidsson et al., 2002; Kokaia and Lindvall 2003; Yamashita et al., 2006), where newly formed neuroblasts migrate from the SVZ towards the ischemic boundary zone (**Fig. 1.15**).

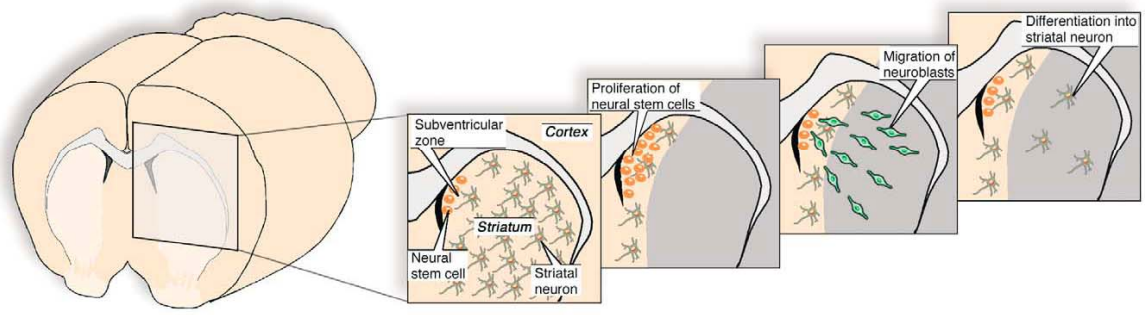

Fig. 1.15. Schematic representation of neurogenesis in striatum following global ischemia. Series of images shows how progenitors migrate towards the ischemic zone. Taken from Kokaia and Lindvall 2003.

In this scenario hypoxia induces a number of factors that might underlie neurogenic response to ischemia including erythropoietin, vascular endothelium growth factor, stem cells factor and heparin-binding epidermal growth factor (Kempermann 2006). The receptors for all these are expressed in the SVZ, making their involvement plausible. Nitric oxide (NO) might also take part in ischemia-induced neurogenesis, because inhibition of inducible nitric oxide synthase (iNOS) or an iNOS null mutation blocked the increase of neurogenesis (Zhang et al., 2005).

1.5.3 Neurogenic and non-neurogenic regions as a source of neural precursors cells

The neurogenic regions of the adult brain are characterized by the presence of a germinative matrix with a significant production of new neurons throughout life. Consequently, the remainder of the brain would be the non-neurogenic regions. There are, however, reports on brain-injury derived neurogenesis outside the classical neurogenic regions, demonstrating that the lack of neurogenic permissiveness can be overcome by a pathological stimuli (Kempermann 2006). However is not completely clear whether pathology assists an endogenous program or actively induces neurogenesis. In line with that, precursors cells populations might be more heterogeneous in their properties than we are inclined to assume.

Several studies provided new insights of other brain regions, such as the neocortex, with the same capacity. Cortical progenitors proliferation has been found in situ after brain injury (Shimada et al., 2010; Zhang et al., 2001), and more importantly, stroke-induced cortical neurogenesis has also described in the adult human brain, even in advanced age patients (Jin et al., 2006; Macas et al., 2006; Minger et al., 2007). Additional studies have specifically reported cortical neurogenesis after stroke (Gu et al., 2000; Jiang et al., 2001), but other studies failed to find new neurons in or around the ischemic cortex (Arvidsson et al., 2002; Parent et al., 2002). Therefore, these results are still a matter of hot debate.

In any case, two conditions have to be fulfilled to make regenerative neurogenesis possible: NPs must be present in the site of injury of regeneration, and the local microenvironment must be switched to neurogenic permissiveness. Another study using targeted apoptosis by direct photolysis of a particular neurons subset,

demonstrate that adult neurogenesis could be induced in adult mammalian non-neurogenic regions and that cell death is enough to trigger it (Magavi et al., 2000).

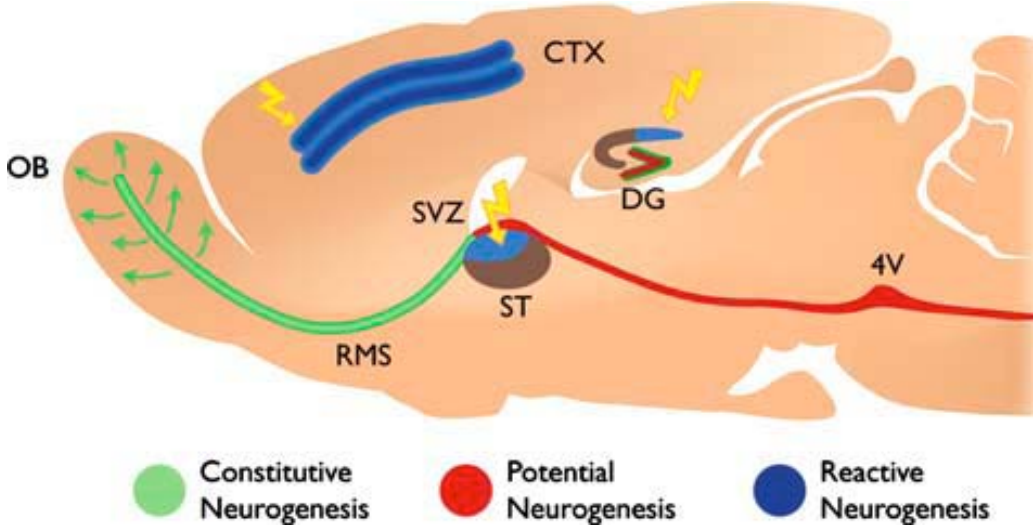

Fig. 1.16. Diagram showing the two constitutively neurogenic regions of the adult mammalian CNS (green; SVZ/olfactory bulb and hippocampal dentate gyrus), and some of the principal regions where populations of neural precursors have been identified (red; potential neurogenesis). The diagram also indicates selected regions in which limited neurogenesis can be induced experimentally (blue; reactive neurogenesis) following cell damage (yellow arrows). CTX: cortex; DG: dentate gyrus of the hippocampus; OB: olfactory bulb; RMS: rostral migratory stream; ST: striatum; SVZ: subventricular zone; 4v: fourth ventricle. Taken from Ortega-Perez et al., 2007.

Nonetheless, whether microglial cells can mediate all these processes and the fate of the newborn neurons is still controversial, but microglia have been strongly pointed out as a neurogenesis regulator (Aarum et al., 2003; Ekdahl et al., 2009; Walton et al., 2006).

1.5.4 Microglial role in neurogenesis

Recently, microglia have been recently recognized as a component of the neurogenic niche, releasing soluble factors that influence positively the proliferation, migration and differentiation of neural precursor cells in the hippocampus and SVZ (Aarum et al., 2003; Deierborg et al., 2010; Walton et al., 2006), and their accumulation in the SVZ has been described after ischemic brain injury (Thored et al., 2009). Nonetheless, whether microglia directs these processes under specific pathological conditions is still a matter of hot debate. Unlike their role in phagocytosis, activated microglia is able to aid in brain repair, providing a potent

neuroprotection (Carson et al., 2006) or acting as a proneurogenic influence that supports the different steps of neurogenesis (Ekdahl et al., 2009). Since microglia activation is a dynamic and complex process in which unique functional patterns can be recognized (Schwartz et al., 2006), it seems not to be proneurogenic or antineurogenic per se. Most likely, the result of that activation is a balance of microglia-secreted molecules that define the net outcome.

The relevance of regenerative processes triggered by brain insults such as traumatic injury, cerebral ischemia or epilepsy, is limited by the poor survival of newly born neurons, which is mainly attributed to the detrimental effect of the inflammatory events sustained by microglia and infiltrating immune cells, determining an unfavorable environment for mature and newborn neurons (Ekdahl et al., 2003; Liu et al., 2007b; Monje et al., 2003). As an example, Arvidsson et al. 2002 have reported that <0.2% of neurons destroyed after MCAO would be replaced by new neurons in the infarcted striatum and even an small percentage in the infarcted cortex. Therefore, activation of endogenous progenitors or reducing apoptosis of the new born neurons can be attractive therapeutic strategies, where microglial cells will play a key role in the process.

1.6 K_{ATP} CHANNELS

ATP-dependent potassium (K_{ATP}) channels play important roles in many cellular functions by coupling cell metabolism to electrical activity (Kline et al., 2009). K_{ATP} channels were first detected in cardiac myocytes and later found in beta-cells (β-cells) of the pancreas, skeletal muscle, neurons, smooth muscle, heart, pituitary, and tubular cells of the kidney. Physiological functions, for example, include insulin secretion in the pancreas, modulation of action potential frequency, and the release of transmitters in neurons, as well as the control of vascular tone in smooth muscle. Moreover, the expression of K_{ATP} channels has also been suggested in microglia previously (McLarnon et al., 2001) (**Fig. 1.18**), and recently demonstrated its role controlling the release of a diversity of inflammatory mediators, such as nitric oxide, IL-6 or TNFα (Ortega et al., 2012a; Virgili et al., 2011).

1.6.1 Physiological relevance and electrical activity

K_{ATP} channels couple metabolism to electrical activity in many tissues by regulating K^+ fluxes across the cell membrane (Akrouh et al., 2009; Kline et al., 2009). Increased energy metabolism leads to channel closure, membrane depolarization and electrical activity. Conversely metabolic inhibition opens K_{ATP} channels and suppresses electrical activity. K_{ATP} channels play a multitude of functional roles in the organism, as initial studies on isolated cells, and more recent analyses of genetically modified mice and patients with mutations in K_{ATP} channel genes. In the brain (Ashford et al., 1990; Levin 2001; Levin et al., 2001; Ohno-Shosaku and Yamamoto 1992), K_{ATP} channels modulate electrical activity and transmitter release (Avshalumov and Rice 2003; Liss et al., 1999; Wang et al., 2004), and protect against seizures (Yamada et al., 2001). In the heart, they are involved in the response to cardiac stress and ischemic preconditioning (Kline et al., 2010; Seino and Miki 2003; Wang et al., 2011). In endocrine cells, they play an important role in the release of hormones, including insulin from pancreatic β-cells (Ashcroft et al., 1984), glucagon from pancreatic alpha-cells (Proks and Ashcroft 2009), and GLP-1 from L-cells (Gribble and Reimann 2003). Consider the case of the pancreatic β-cell (**Fig. 1.17**). At substimulatory glucose concentrations, K_{ATP} channels dominate the plasma membrane conductance. The generated outward K^+ current hyperpolarizes the β-cell membrane, preventing electrical activity and insulin secretion. Elevation of the plasma glucose concentration stimulates glucose uptake and metabolism by the β-cell, causing an increase in ATP and a concomitant MgADP decrease. These changes in adenine nucleotide concentrations close K_{ATP} channels (Ashcroft et al., 1984). As a consequence, the membrane depolarizes by opening voltage-gated Ca^{2+} channels, which initiate Ca^{2+}-dependent electrical activity, Ca^{2+} influx and insulin release (Ashcroft 2005). Thus the activity of the K_{ATP} channel controls whether β-cell secretes insulin or not.

Despite its well studied function in β-cell, the expression of K_{ATP} channels has also been suggested more recently in microglia (McLarnon et al., 2001) (**Fig. 1.18**), and has been demonstrated its role controlling the release of a diversity of inflammatory mediators, such as nitric oxide, IL-6 or TNFα (Ortega et al., 2012a; Virgili et al., 2011).

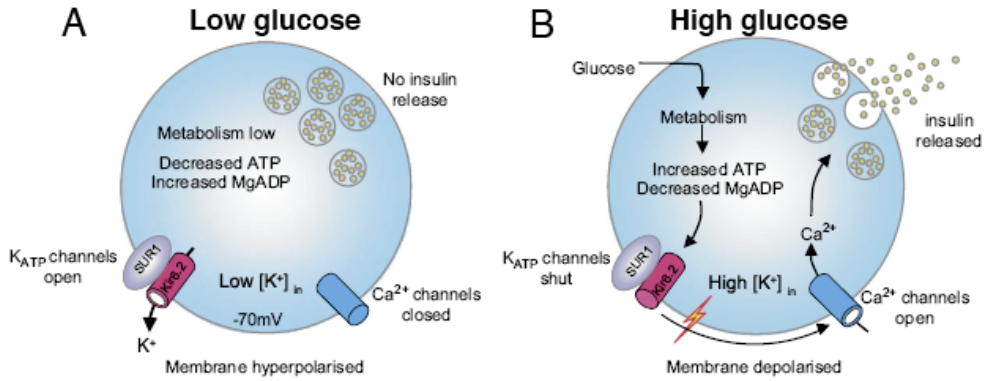

Fig. 1.17. Stimulus–secretion coupling in pancreatic β-cells. (A) K_{ATP} channels are open when extracellular glucose, and thus β-cell metabolism, is low (hyperpolarized). This keeps voltage-gated Ca^{2+} channels closed, so that Ca^{2+} influx remains low and insulin secretion is inhibited. (B) When extracellular glucose increases, metabolism generates ATP at the expense of MgADP, thereby closing K_{ATP} channels (depolarization), and K^+ is accumulated inside the cell, opening of voltage-gated Ca^{2+} channels, Ca^{2+} influx and exocytosis of insulin. Adapted from Proks and Ashcroft 2009.

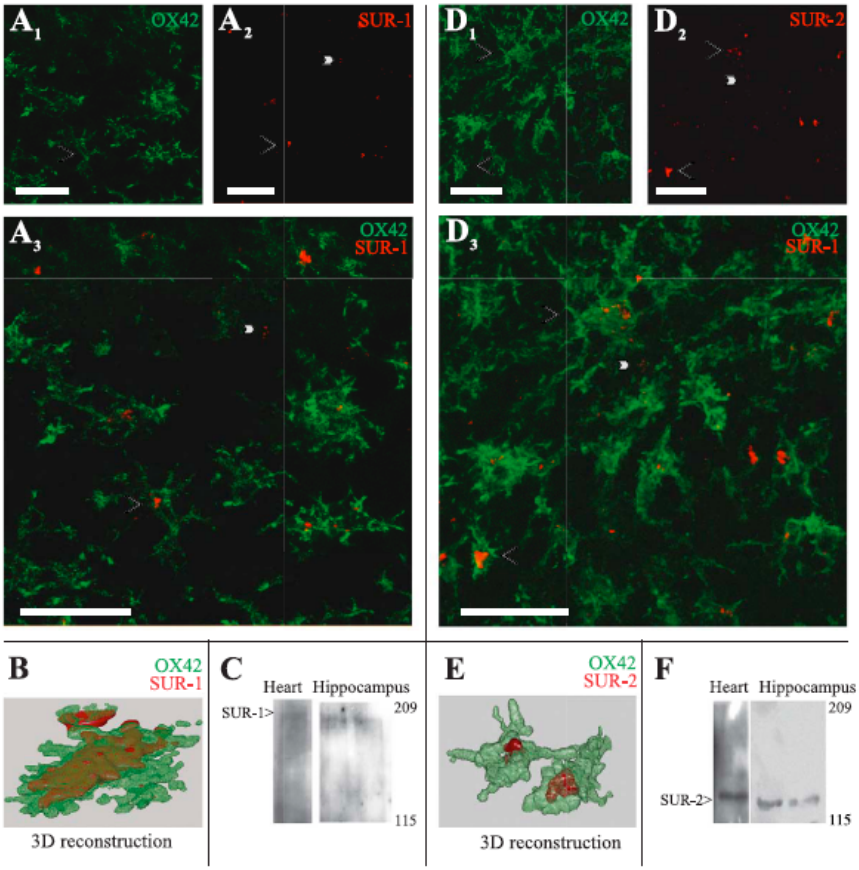

Fig. 1.18. Expression of sulfornylureas receptor (SUR) isoforms in AMPA-lesioned rat hippocampal formation (HF). (**A1, D1**) Representative confocal OX-42 immunofluorescence image showing amoeboid activated microglia at the lesioned HF (arrowhead) expressing SUR-1 (**A2**) or SUR-2 (**D2**). (**A3, D3**) Merge of A and D images denote colocalization. (**B, E**) 3D reconstruction of a typical microcyte verifies that SUR-1 or SUR-2 staining is present in the microglia in a membrane-compatible localization. (**C**) Illustrative Western blot with anti-SUR-1 antibody in human heart and rat hippocampal extracts revealing glycosilated SUR-1 band. (**F**) Illustrative Western blot with anti-SUR-2 antibody in human heart and rat hippocampal extracts revealing the expected band at 140 kDa. Scale bars: 40 µm. Taken from Ramonet et al., 2004.

1.6.2 Protein architecture of the K_{ATP} channel

K_{ATP} channels are assembled as a hetero-octameric complex (Clement et al., 1997; Mikhailov et al., 2005; Proks and Ashcroft 2009; Wheeler et al., 2008) from two structurally distinct subunits: the pore forming inwardly rectifying K^+ channel (Kir) subunit 6.1 or 6.2 and the regulatory sulfonylurea receptor (SUR). SURs, like all other ATP-Binding Cassette (ABC) transporters, contain two transmembrane domains (TMD1 and TMD2) and two cytoplasmic domains (Nucleotide Binding Folds 1 and 2, NBF1 and NBF2); in addition, it possesses a N-terminal transmembrane domain (TMD0), which mediates SUR-Kir6 interactions (Mikhailov et al., 2005). Therefore, the channel is a functional octamer of four Kir6 subunits, and each Kir6 subunit is associated with one SUR protein (Clement et al., 1997) (**Fig. 1.19**).

While ATP inhibits the K_{ATP} channel by direct binding to the cytoplasmic domains of Kir6, SUR is responsible for channel regulation by other ligands, including high-affinity inhibition by sulfonylurea drugs (Gribble et al., 1997; Mikhailov et al., 2001) stimulation by potassium channel openers (KCO's), and stimulation by Mg-nucleotides (Ashcroft and Gribble 1998; Nichols 2006).

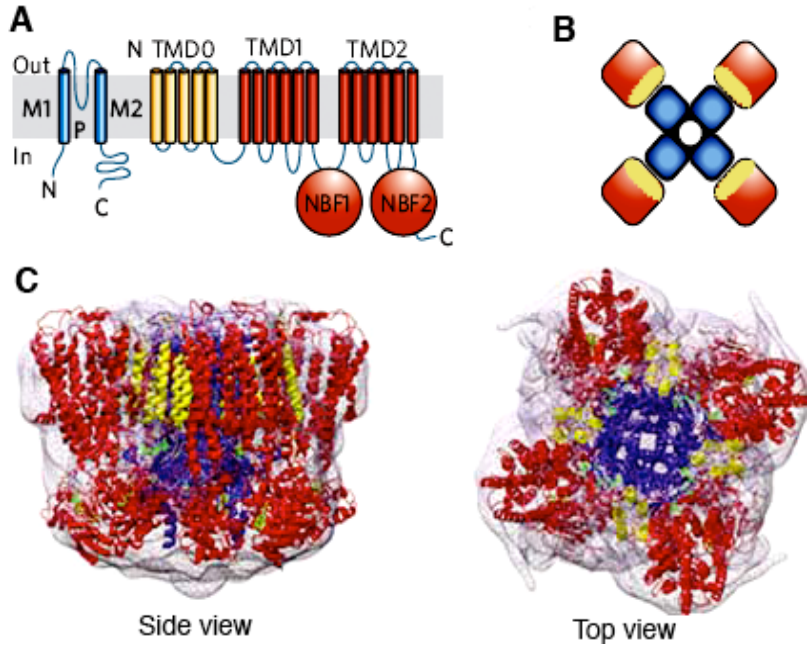

Fig. 1.19. Topography of the K_{ATP} channel.

A) Kir6 subunits generate the channel pore and sulfonylurea receptor (SUR) subunits generate the regulatory subunit. TMD, transmembrane domain; NBF, nucleotide-binding fold; M1, M2, transmembrane helices; P, pore.

B) The channel is a functional octamer of four Kir6 subunits, and each subunit is associated with one SUR subunit.

C) Location of molecular models within the 3D structure, ATP molecules are shown in green. Adapted from Nichols 2006.

1.6.3 Assembly and trafficking

K_{ATP} channels are assembled in the Endoplasmic Reticulum (ER) from Kir6 and SUR subunits. Each subunit possesses an ER retention motif, RKR, which prevents trafficking of mismatched subunits to the membrane: in Kir6.2, it is located in the C-terminus, whereas in SUR1 it is located in the cytoplasmic loop between TMD1 and NBF1 (residues 648–650) (Kline et al., 2009; Zerangue et al., 1999). In the fully-assembled K_{ATP} channel complex, each retention signal is apparently masked by the other subunit, and the channel can exit the ER (Zerangue et al., 1999). Ablation of this motif by mutation, or by truncation of the C-terminus in the case of Kir6.2 facilitates trafficking of either subunit alone. Trafficking of SUR1 to the membrane is also dependent on N-linked glycosylation, and because of that, SUR1 migrates as multiple molecular weight species on electrophoresis from cell lysates: the lower molecular weight species corresponds to the immature, core-glycosylated ER fraction, and the higher molecular weight species correspond to the mature, fully-glycosylated plasma membrane fraction (Masia et al., 2007).

1.6.4 Channel gating

The octameric structure of the K_{ATP} channel means that channel regulation by nucleotides is extremely complex. There are four inhibitory ATP-binding sites per channel (one on each Kir6.2 subunit) and eight stimulatory Mg-nucleotide-binding sites on SUR (Clement et al., 1997). Channel activity is therefore determined by the balance between the effects of nucleotides at each of these sites. Several ligands affect K_{ATP} channel activity. ATP (with or without Mg^{2+}) inhibits, and phosphatidylinositol-4,5-bisphosphate (PIP_2) activates, by direct interaction with Kir6.2 subunits. Sulfonylureas inhibit, and K^+ channel-opener drugs activate, by interaction with the SUR subunit. In addition, in the presence of Mg^{2+}, ATP and ADP can activate the channel through interaction with the NBFs of SUR (**Fig. 1.20**). Inhibition by ATP binding to Kir6.2 and activation by Mg-nucleotides is almost certainly the primary physiological regulatory mechanism (Nichols 2006). The kinetics of this particular channel is extremely complex because the multimeric structure of the channel means that there will be a large number of kinetic states.

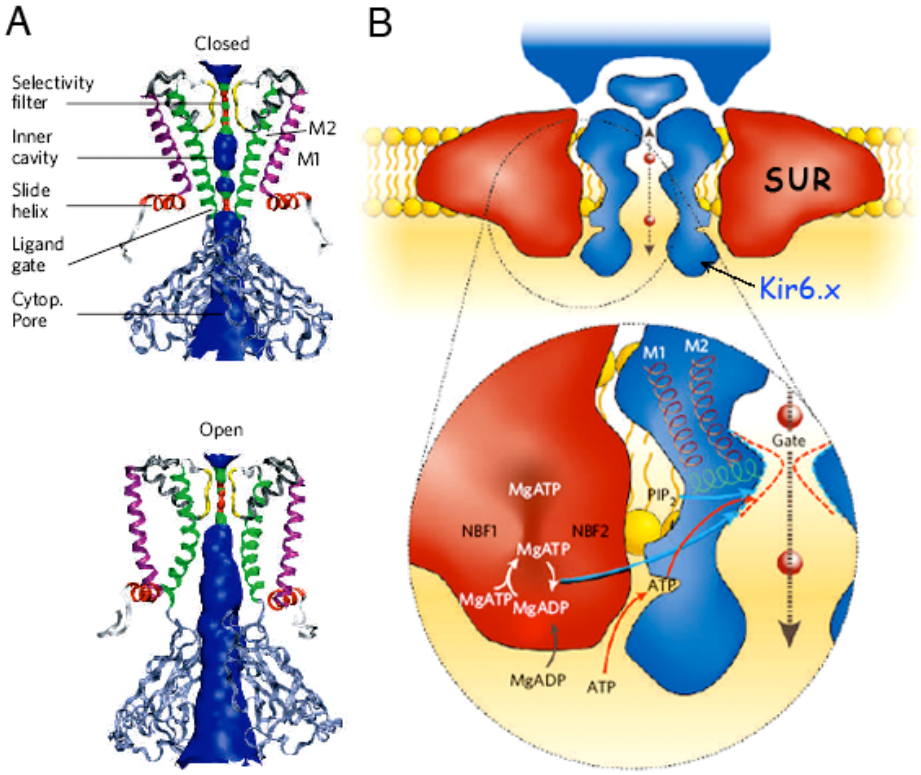

Fig. 1.20. ATP-dependent gating and the nucleotide regulation of K_{ATP} activity. A) A model inward rectifier K+ (Kir) channel showing potential gating states. Closed and open structures modeled on two-dimensional crystals of KirBac3.1 are shown in two different conformational states. The blue volume represents free access of water. B) The metabolically controlled gate of the channel is located at the cytoplasmic end of the inner cavity. PIP_2 gives an energetic pull to open channels, and ATP provides the push to close the ligand-operated gate, perhaps through the physical link provided by the 'slide helix' (green). MgATP binds to each of the ATP-binding sites that are formed at the interface between nucleotide-binding folds NBF1 and NBF2 in each sulfonylurea receptor (SUR) subunit. ATP hydrolysis at the second site results in a conformational 'activated' state that is transduced to an 'override' of ATP inhibition at the Kir6.2 subunit. The 'activated' state persists through MgADP dissociation, and can be maintained by MgADP rebinding. Taken from Nichols 2006.

1.6.5 Channelopathies

The crucial role of the K_{ATP} channel in β-cell is illustrated by the functional effects of mutations in K_{ATP} channel genes. Loss-of-function mutations that result in permanent K_{ATP} channel closure produce β-cell depolarization, persistent insulin secretion even when blood glucose is low, and thereby congenital hyperinsulinism (Ashcroft 2005). Conversely, gain-of-function mutations in K_{ATP} channel genes give rise to neonatal diabetes by keeping the β-cell hyperpolarized and preventing insulin secretion (Ashcroft 2005; Proks and Ashcroft 2009). Most of these mutations lead to neonatal diabetes, but in some patients diabetes may present later, even in adult life. Because K_{ATP} channels are found in many other tissues, both gain and

loss-of-function mutations can cause extrapancreatic effects. These are most dramatic in the case of severe activating mutations, which can result in developmental delay, epilepsy, muscle weakness, dysmorphic features and neonatal diabetes, a condition known as DEND syndrome (Ashcroft 2005; Proks and Ashcroft 2009). On the other hand, dysregulation of SUR assembly and trafficking has important physiological consequences, as evidenced by mutations that cause retention of SUR1 in the ER or in the Golgi, leading to reduced channel expression and causing persistent hyperinsulinemic hypoglycemia of Infancy in humans. Some mutations can be fully or partially rescued by ablation of the RKR motif. Others can be rescued by sulfonylurea treatment, which reduces degradation of the mutant protein via the ubiquitination-proteasomal degradation pathway (Masia et al., 2007).

1.7 K_{ATP} channel pharmacology

In recent years, potassium channels in general and K_{ATP} channels in particular have attracted increasing interest as targets for drug development. Their pivotal role in a plethora of physiological processes has been underscored by recent discoveries linking potassium channel mutations to various diseases. Second generation of potassium channel openers (KCOs) or potassium channel blockers (KCBs), which differ from their predecessors by a significantly improved *in vitro* or *in vivo* selectivity, broaden the chemical diversity of K_{ATP} channel ligands (Lawson 2000). Despite this indisputable progress, however, a lot of work remains to be done to fully exploit the pharmacological potential of K_{ATP} channels and their KCOs or KCBs ligands. Considering the unique role that K_{ATP} channels play in the maintenance of cellular homeostasis, KCOs add to existent pharmacotherapy with potential in promoting cellular protection under conditions of metabolic stress. Preclinical evidence indicates a broad therapeutic potential for KCOs, for example, in hypertension, cardiac ischemia, asthma, or urinary incontinence to mention a few.

On the other hand, sulfonylureas inhibit K_{ATP} channels by interacting with two drug-binding sites on the K_{ATP} channel (Gribble et al., 1997). The primary effect is mediated via a high-affinity binding site that lies on SUR. A second, low-affinity binding site lies on Kir6.2; however, this site is not clinically relevant as the

concentrations required for inhibition at Kir6.2 are much higher than those found in the plasma of patients treated with this antidiabetic drugs. Sulfonylureas can be divided into two major groups with respect to their selectivity for different types of sulfonylurea receptor (Gribble and Reimann 2003). The first group produces high-affinity block only of K_{ATP} channels containing SUR1 receptors, whereas the second group shows a similar affinity for all SUR isoforms (i.e. it is non-specific). To interpret these findings, a two site model for the interaction of sulfonylureas with SUR has been proposed, in which some sulfonylureas interact with a single site that is common to all SURs, whereas other sulfonylureas bind both to this site and to an SUR1-specific site (Gribble and Reimann 2003; Gribble et al., 1997). Unlike the nucleotide-binding sites on Kir6.2, little is known about the location and structure of the high affinity sulfonylurea-binding site. However, residues in both the third (between TMs 5–6) and eighth (between TMs 15 and 16) cytosolic loops are involved, suggesting the binding site involves multiple parts of the protein (Enkvetchakul and Nichols 2003; Mikhailov et al., 2001).

The K_{ATP} channel is also the site of action of the sulfonylurea drugs. Sulfonylureas are oral hypoglycemic agents widely used in the treatment of type II diabetes mellitus (Melander et al., 1990). Drugs such as Glibenclamide (Gbc) (**Fig. 1.21)** bind with subnanomolar or nanomolar affinity and are potent inhibitors of SUR1-regulated channel activity (Simard et al., 2008). SUR1-regulated channels are exquisitely sensitive to changes in the metabolic state of the cell, responding to physiologically meaningful changes in intracellular ATP concentration by modulating channel open probability.

Moreover, analysis of radiolabeled Gbc binding to the SUR subtypes reveals that occupation of one of the four SUR sites per channel complex is sufficient for the closure of K_{ATP} channels (Dörschner et al., 1999).

Giving the fact that SUR1-regulated channels are exquisitely sensitive to changes in the metabolic state of the cell, and that are sensing the environment, the expression of K_{ATP} channels in activated microglia, will couple cell energy to membrane potential may then be critical in determining, at least in part, their participation in the pathogenic process. If this is the case, when K_{ATP} channel is blocked with Gbc, a highly selective blocker of the channel, microglia membrane

potential will decrease rendering the cell more sensitive to external signals and enabling microglia rapidly respond to neuronal damage.

Sulfonylurea receptors (SURx)—their principal constitutive locations and blockers			
	SUR1	SUR2A	SUR2B
Principal constitutive locations[a]	Pancreatic β cell hippocampus neocortex olfactory bulb cerebellum hypothalamus substantia nigra	Cardiac muscle skeletal muscle	Smooth muscle vascular smooth muscle
Blockers[b]			
Glibenclamide	0.13–4.2	27–45	42–166
Glimepiride	3.0	5.4	7.3
Repaglinide	5.6–21	2.2	2

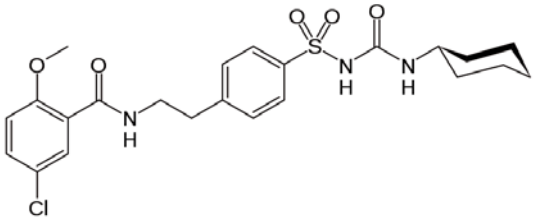

Fig. 1.21. a) Only selected constitutive locations with high levels of expression are listed. b) Only selected blockers that exhibit long 'off-time' constants and that have been used in preclinical or clinical trials related to CNS injury are listed; values are for $IC_{(50)}$ for inhibition of ion channel current in nM. Taken from Simard et al., 2008. Left) Chemical structure of Gbc ($C_{23}H_{28}ClN_3O_5S$**).**

1.8 THERAPEUTIC STRATEGIES

Ischemic brain injury is a complex mechanism that involves energy failure, excitotoxicity, the accumulation of ROS, programmed cell death and inflammatory processes. Thus, the main targets to treat ischemic stroke include: restore the cerebral blood flow from the ischemic region, restore the energy metabolism failure and to enhance the neuroprotective mechanisms.

1.8.1 Cerebral blood flow can determine the fate of ischemic tissue

Ample evidence supports the concept that blood flow is one major determinant of the fate of ischemic tissue. A given change in level of blood flow leads to a specific metabolic alteration and pathological outcome (Dirnagl et al., 1999). Various agents have been used in clinical trials to restore cerebral blood flow. All of the agents designed to restore blood flow are inappropriate for treating hemorrhagic stroke because of the danger of exacerbation of cerebral bleeding. In fact, most of the drugs that restore blood flow are associated with an increased risk of hemorrhage particularly when administered late (>6 hours). The drugs used to restore blood flow can generally be grouped into antithrombotics, antiplatelet agents, fibrinogen

depleting agents, or thrombolytics. Nowadays the early blood flow recovery by recombinant tissue plasminogen activator (rt-PA) is the only thrombolytic pharmacological therapy approved in humans, and has given good results so far (Lo 2008). Thrombolytic treatment with rt-PA is effective because it restores cerebral blood flow in ischemic regions with the aim of preventing or minimizing cell damage, thus improving its fate. After a brief ischemic episode, brain cells are able to restore their ionic homeostasis simultaneously with an energetic restoration (Ekholm et al., 1993). Nonetheless, if the ischemia is long enough, the thrombolytic treatment will be detrimental for cells, because it triggers damage by reperfusion (Carmichael 2006; Spranger et al., 1998).

Recent developments in our understanding of the pathophysiological events that follow acute ischemic stroke suggest an important role for angiogenesis in this process, which, through new blood vessel formation, results in improved collateral circulation and may impact on the medium-to-long term recovery of patients. Therefore, angiogenesis is a key feature of ischemic stroke recovery and neuronal post-stroke re-organization, in particular in the ischemic boundary zones or penumbra region adjacent to the infarct, where partially affected neurons exposed to intermediate perfusion levels have the capability of survival if perfusion is maintained or normalized

1.8.2 Energy metabolism and oxidative stress as determinants of the fate of ischemic cells

As compromised energy metabolism in the penumbra contributes to the evolution of cerebral infarction, many classic neuroprotectants are membrane stabilizers that preserve intracellular ATP levels (Liu and Levine 2008). Accumulating evidence suggests that energy state, or the ATP level, determines the fate of ischemic tissue and the pathways for cell survival and cell death. Energy status has been shown to correlate well with cell survival and recovery in rat and *in vitro* models of ischemia and hypoxia (Ginsberg 1997) in hippocampal slice cultures and primary cortical astrocytic cultures (Yu et al., 2009). Differential ATP levels also determine the pathway to apoptosis. On the other hand, after cerebral ischemia, mitochondrial

dysfunction can ensue as a result of oxidative stress, energy failure and the disruption of cellular calcium homeostasis; this is considered to be a crucial event that triggers the execution of programmed cell death in neurons (**Fig. 1.22**).

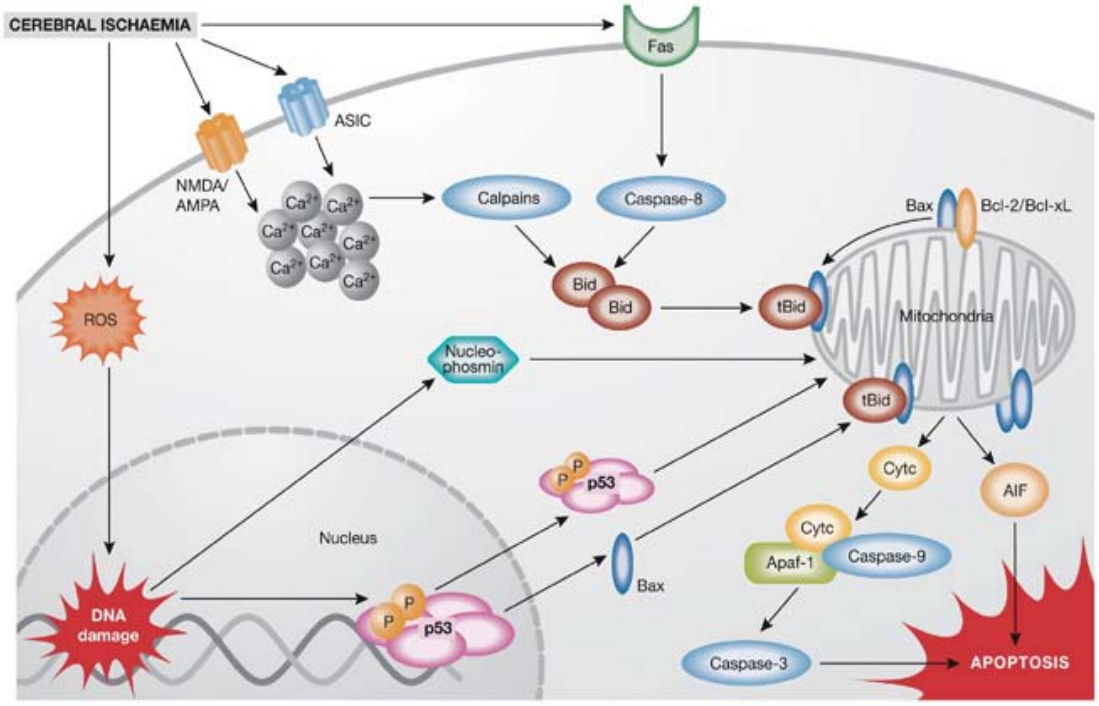

Fig. 1.22. Mechanisms of ischemic-derived neuronal cell death. Ischemic neuronal death is mediated by a plethora of intracellular mechanisms, such as increased calcium levels, ROS, DNA damage and mitochondrial dysfunction. Post-ischemic cytotoxic calcium influx is mediated through the stimulation NMDA or AMPA receptors. Taken from Culmsee and Krieglstein 2007.

An important regulatory step of this process occurs at mitochondrial membranes, where members of the B-cell leukemia/lymphoma 2 (Bcl-2) family of proteins either promote (Bax, Bid, Bad and Bim) or prevent (Bcl-2 and Bcl-xL) the formation of outer membrane pores that cause mitochondrial dysfunction and allow the release of pro-apoptotic factors, such as cytochrome *c* and apoptosis-inducing factor (AIF), from the mitochondrial intermembrane space. In this regard, although caspase activation has been widely documented in ischemic brain tissue in various stroke models, increasing evidence suggests a substantial role for caspase-independent pathways in ischemic neuronal cell death, which involve the mitochondrial release of AIF. It has been described that low levels of AIF, resulted in a pronounced reduction of neuronal cell death in models of brain trauma and cerebral ischemia (Culmsee and Krieglstein 2007).

1.8.3 Neuroprotective strategies

The cytotoxic accumulation of intracellular calcium has been established as a crucial step in ischemic neuronal cell death (Orrenius et al., 2003). Until recently, it was widely accepted that cytotoxic intracellular calcium overload after ischemia is mediated mainly through the stimulation of glutamate receptors or voltage-dependent calcium channels. That's why in the last years scientist made an effort to develop new therapeutic strategies focused in calcium channel antagonist, glutamate receptor antagonists GABA receptor antagonist or voltage-dependent calcium channels antagonists.

The SUR1-regulated K_{ATP} channel has been extensively reviewed (Aguilar-Bryan and Bryan 1999; Campbell et al., 2003; Seino and Miki 2003). The neuronal K_{ATP} channel has been directly linked neuroprotection because become activated in ATP-depleted metabolic states such as hypoxia and may contribute to protection against energy-consuming generalized seizures (Ballanyi 2004; Yamada and Inagaki 2005). Sulfonylureas such as Gbc can depress hypoxia-induced hyperpolarization in hippocampal and neocortical neurons, thereby antagonizing the neuroprotective function of these channels. However, K_{ATP} channels are believed to fully exert their protective role only in very limited severities of hypoxic challenge just above the critical transition, apparently delaying but ultimately not preventing major depolarization, which probably limits their overall contribution to neuroprotection (Ballanyi 2004; Yamada and Inagaki 2005).

Nonetheless, functional SUR1-regulated non-selective cationic ($NC_{Ca\text{-}ATP}$) channels have been also described in astrocytes (Simard et al., 2006), and blockade of SUR reduce cerebral edema and infarct volume and decrease mortality in experimental stroke models (Simard et al., 2010). A retrospective study has also shown that patients with diabetes mellitus taking Gbc have a better neurological outcome (Kunte et al., 2007), although this finding has recently been challenged (Favilla et al., 2011). Binding sites for sulfonylurea and related drugs are accessed via the lipid layer. For weak acids such as Gbc it is thus the un-ionized form that is active. As a result, both drug-binding and drug-induced channel block are increased at acidic pH. An increase in potency at low pH is observed not only with K_{ATP} channels, but also with SUR1-regulated $NC_{Ca\text{-}ATP}$ channels. Decreasing the pH from

7.4 to 6 duplicated the magnitude of channel block by 50 nM in the neurons located in the core of the ischemic brain (Simard et al., 2006). Moreover, astrocytes from the ischemic inner zone of the gliotic capsule, decreasing the pH from 7.4 to 6.8 shifts the EC_{50} for Gbc from 54 to 6 nM. This effect of pH on apparent drug potency is believed to enhance drug effect at the acidic pH characteristic of ischemic or injured CNS tissues (Nedergaard et al., 1991).

1.8.4 Neurogenesis and neurorestorative therapy: oxidative stress and inflammation

Hopes were raised for stem-cell directed stroke therapy after it was shown that pluripotent stem cells had protective effects and enhanced endogenous neurogenesis after ischemic brain injury (Zhang et al., 2005). Several groups reviewed therapeutic strategies that support adult neurogenesis by enhancing protein levels of basic fibroblast growth factor (bFGF), epidermal growth factor (EGF), granulocyte colony-stimulating factor (G-CSF) and brain-derived neurotrophic factor (BDNF). Furthermore, endogenous regeneration and functional improvement were achieved by compounds that are clinically established in other therapeutic categories, for example, erythropoietin, HMG-CoA reductase inhibitors, and phosphodiesterase-5 inhibitors, enhanced angiogenesis and neurogenesis in experimental models of stroke, even when applied more than 24 h after the onset of ischemia (Arboix 2007; Wiltrout et al., 2007; Zhang et al., 2005). Because of the typical size of the lesion and the complexity of the destroyed brain structure, an unfeasible approach is cell transplantation to reconstruct the entire lost structure. Cell therapy however, might aid in retaining tissue that would otherwise succumb to secondary loss and might provide trophic or other support to the spared structures. Since this benefit can also be obtained from internal resources, a promising long-term therapeutic strategy might be to promote endogenous attempts for regeneration to improve outcome after stroke (Kempermann 2006).

It is also noteworthy to mention that during reperfusion, ROS contribute to damage neurons when antioxidant defense mechanisms are optimal. Superoxide, hydrogen peroxide, and hydroxyl radicals are responsible for damaging membranes and degrading deoxiribonucleotic acid (DNA). In experimental models, agents such

as vitamin E, glutathione, superoxide dismutase, iron chelators, lazaroids, NPY-059, and catalase have been tested as free radical scavengers. However until now none of them showed efficacy (Haley et al., 1995; Johnston et al., 1998; Yamaguchi et al., 1998).

In conclusion, inflammatory response, the neurovascular unit, neurogenesis, angiogenesis, and cell-death pathways are the main targets for stroke therapy. Promising future approaches will combine high-throughput technologies, such as proteomics, genomics and siRNA screening, to investigate further mitochondrial cell-death pathways, systemic immune responses and, in particular, reversible phosphorylation. However, more stringent criteria in the performance, reporting and analysis of animal data are clearly required to identify the most efficient therapeutic strategies to be successfully transferred into the clinic. Consequently, the standard view of neuroprotection, which has long been exclusively neurocentric, is no longer accepted. Instead it has been replaced by a more integrative approach that recognizes the importance of dynamic interactions between cells that form the 'neurovascular unit'. That is, endothelial cells, microglia, astrocytes, and neurons.

1.9 HIPOTHESIS

Fast activation of microglia in response to neuronal damage requires the rapid availability of a large amount of energy to trigger diverse cytotoxic or neuroprotective signals. The expression of K_{ATP} channels in activated microglia may then be critical in determining, at least in part, their participation in the pathogenic process. Given the analogy with β-cells, K_{ATP} channel blockade in microglia would response faster and more efficiently to the external signals released after brain injury. If true, blockade of microglial K_{ATP} channel with low doses of Gbc after cerebral ischemia would enhance ischemia-induced neurogenesis in the SVZ, leading thus to an improved functional outcome.

In this scenario, controlling the microglial activation and the inflammatory mediators released to the brain parenchyma may offer clinical therapeutics for short-term inflammation-related beneficial effects that include potentiation of neurogenesis.

Chapter 2.
AIMS

1- To assess whether the microglia BV2 cell line express functional K_{ATP} channels, and whether its blockade with glibenclamide modulates the reactivity of BV2 microglia.

2- To investigate the motor and behavioral effect of KATP channel blockade with low doses of glibenclamide in a rat model of tMCAO. Then, to study the correlation of these functional effects with the neuroprotective actions of glibenclamide at morphological and histological levels.

3- To investigate whether glibenclamide modifies the intrinsic neurogenesis and the fate of newborn neuroblasts triggered by tMCAO in rats.. Also, to assess whether the ischemia-induced neurogenesis correlates with the behavioral outcome and the cellular response in terms of neuroprotection, lesion volume and angiogenesis.

4- To examine *in vitro* the effect of microglia K_{ATP} channel blockade on neuronal precursors cells using the neurosphere assay. This aim included to identify at least one microglia soluble factor whose release is controlled by K_{ATP} channel and that enhances SVZ neurogenesis

Chapter 3.
MATERIAL AND METHODS

3.1 Animals

For Results block I: Adult male Wistar rats (3 months old, body weight 250-300 g at the beginning of the study) were obtained from Charles River Laboratories (Sulzfeld, Germany). They were kept on a 12 hours/12 hours day and night cycle and housed with free access to food and water. Animals were handled according to European legislation (86/609/EEC). All efforts were made to minimize the number of animals used and their suffering. Experiments were conducted according to the National Institutes of Health (NIH) guidelines for the care and use of laboratory animals. All procedures were approved by the Ethics Committee of the Universitat de Barcelona, in accordance with the regulations established by the Catalan government (*Generalitat de Catalunya*).

For Results block II: Male Wistar rats (3 months old and weighing between 250 and 300 g at the beginning of the study; National Laboratory Animal Centre, Kuopio, Finland) were used. They were kept on a 12 h/12 h day and night cycle and housed individually with free access to food and water (20±1°C). Animals were handled following European legislation (86/609/EEC) and all efforts were made to minimize the number used and animal suffering. The Ethics Committee of the University of Kuopio and the Provincial Government of Kuopio approved the *in vivo* study. Experiments were conducted according to the National Institutes of Health (NIH) guidelines for the care and use of laboratory animals. All procedures were approved by the Ethics Committee of the Universitat de Barcelona, in accordance with the regulations established by the Catalan government (*Generalitat de Catalunya*).

For Results block III: Adult animals (3–4 month old) C57BL/6 mice and the enhanced green fluorescent protein (eGFP)–colony stimulating factor 1 receptor (Csf1r) transgenic mice, in which the Csf1r promoter drives expression of eGFP in cells of macrophage lineage, were used in this study. Sibling animals were collected and individually genotyped by polymerase chain reaction (PCR) as described previously (Knudson et al., 1995). All experiments were conducted according to the Australian Code of Practice for the Care and Use of Animals for Scientific Purposes and with approval from the University of Queensland Animal Ethics Committee.

3.2 MCAO surgery and drug delivery

Focal ischemia was produced by tMCAO using the intraluminal filament technique (Van Groen et al., 2005). Briefly, rats were anesthetized by 5% halothane (in 70% N_2O / 30% O_2). A surgical depth of anesthesia was maintained throughout the operation with 0,5 to 1% halothane, delivered though a nose mask. The right common carotid artery was exposed by a longitudinal midline incision in the ventral view of the rat neck (**Fig. 3.1. A** and **B**). Submaxilar glands and omohyoideus and sternohyoideus muscles were separated by blunt dissection and the right common carotid and external carotid arteries were dissected. Then, the internal carotid artery was exposed and dissected, being especially careful with vagal nerve management and dissection from carotid body, until the pterygopalatine artery origin can be seen (**Fig. 3.1. B).**

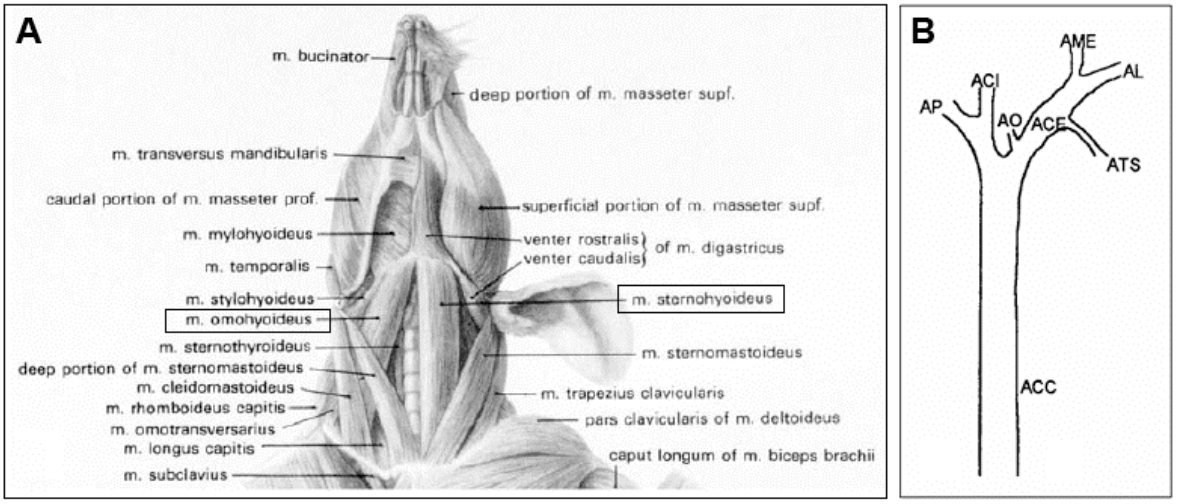

Fig. 3.1. A) Muscle anatomy of the rat neck (ventral view). **B)** Right ventral vascular anatomy of the rat neck. ACC: common carotid artery; AP: pterygopalatine artery; ACI: internal carotid artery; ACE: external carotid artery; AO: occipital artery; AME: external maxilar artery; ATS: upper thyroid artery.

To occlude blood flow to the right MCA territory, a dissection and coagulation of the first two branches of the external carotid artery was done: upper thyroid and occipital arteries. Two ligatures (6-0 braided silk) were placed on the external carotid artery above these coagulated branches, and the artery was cut between them. The result is a stump of the external carotid artery. Then the pterygopalatine artery is ligated near its origin (proximal), as a result, we obtain a transient blood flow interruption between common carotid and internal carotid arteries, which includes

the external carotid artery stump, placing two microvascular clips: one on common carotid artery and another on the initial segment of the internal carotid artery. When the blood flow is interrupted, a small incision was made in the distal portion of the stump and a heparinized nylon monofilament (0.25 mm diameter, tip blunted), was introduced inside (21-23 mm), placing a silk ligature to prevent bleeding when the microvascular clips were removed (

Fig. 3.2. A). MCA occlusion is accomplished pushing the filament until its rounded tip reaches the origin of the MCA origin in the Willis Circle, where a resistance to advance was felt. The filament was held in place by tightening a suture around the internal common carotid artery and placing a microvascular clip around the artery. Corticostriatal damage was induced by an occlusion of the MCA of 60 min (***Results block I***) or 90 min (***Results block II***), and then the MCA blood flow was restored by removal of the filament, and the external carotid artery was permanently closed by electrocoagulation. The wound was closed, disinfected, and the animals were allowed to recover from anesthesia. To balance the MCAO groups the neurological symptoms were assessed before drug administration using two tests: contralateral rotation/circling behavior and contralateral forelimb/hindlimb impairment (lack of limb withdrawal when hanging over the edge of a table). Animals with no behavioral impairment were excluded from the study.

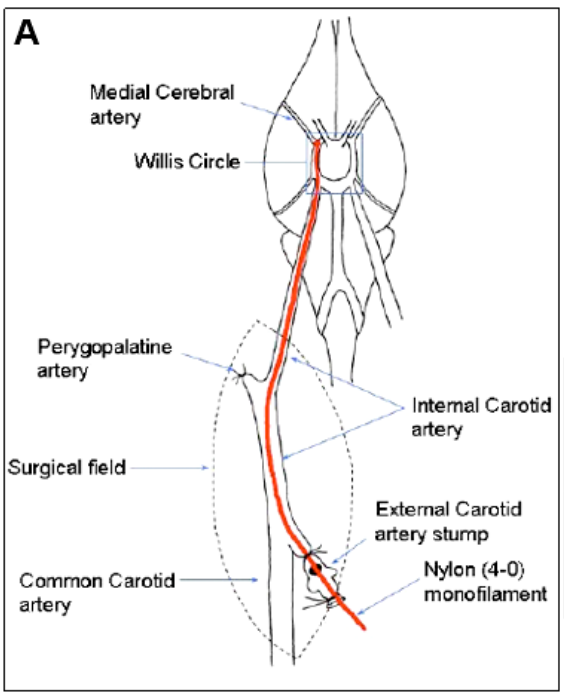

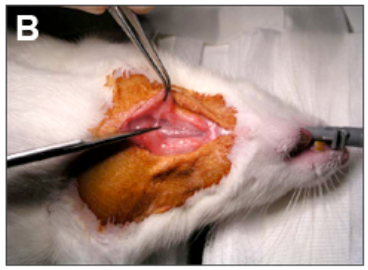

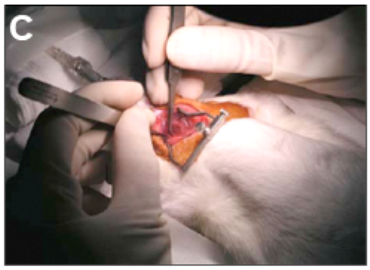

Fig. 3.2. A) Vascular anatomy of right ventral zone of rats' neck and base of the encephalon, showing the introduction of the intraluminal suture surgical sequence where a discontinuous line defines the surgical field. **B)** Image of the rats' neck skin incision. **C)** Image of the carotid artery dissection.

For the assessment of Gbc bioavailability, permanent MCAO was performed following the same procedure but without the filament being removed. In all cases, body temperature was monitored and maintained above 36.5ºC with a homoeothermic blanket system. Successful tMCAO was verified by assessing sensory motor impairment and by measuring infarct volumes at the end of the study. To prevent dehydration, all animals received a daily i.p. injection of saline (4 ml per rat). Animals showing 0-lesion (no detectable infarct) or hemorrhagic transformations (visual inspection) were excluded from the study.

3.3 Calculation of glibenclamide bioavailability

To calculate whether Gbc can reach the brain of MCAO rats, 3 animals received an i.p. injection of 100 µCi [^{3}H]Gbc (43.3 Ci/mmol; Perkin Elmer, Waltham, MS) in a volume of 0.9 ml/rat 16 h after permanent MCAO induction. The surgery approach was the same as described above, but without withdrawing the filament. Two hours later (time point 18 h after MCAO induction), they were anesthetized with isofluorane and transcardially perfused with 200 ml of 0.1 M phosphate buffer saline (PBS, pH 7.4) (**Fig. 3.3A)**. Briefly, animals were placed on its back, and pin out all four limbs at the feet. Using the forceps, we lifted the skin and body wall in the peritoneal area, using the blunt-end scissors we cut through the tent and we enter the body cavity. Then, we extended this opening laterally, and then straight up each side with two long cuts. Afterwards, we opened the rib cage to just aside the lungs, then we cut through the diaphragm by lifting the sternum and placing one blade of the scissors on either side of the membrane. Pinning the loose flap of skin out of the way we released the heart by tearing any connective tissue with the forceps. We turned on the PBS before placing the needle into the left ventricle and holding the heart gently with the blunt forceps. While supporting the heart with the needle and hemostats, we made a small incision in the right atrium (**Fig. 3.3B)**. Brains were then quickly removed (the right and left hemispheres collected separately), frozen in liquid N_2 and stored. Tissue samples were manually homogenized in 7 volumes of ice-cold 50 mM Tris/HCl (pH 7.6) and radioactivity was counted in triplicate. 100 ml homogenate was diluted in 10 ml scintillation cocktail and mixed for 2 hours.

Specific ^{3}H emission was counted in each solution for 60 seconds using a LS3801 Liquid Scintillation Counter (30% efficiency). Two blank samples (non-radioactive tissue homogenate and distilled water) were also included in the study. The Bradford method was used to calculate the protein content of each sample (**Fig. 3.3A)**.

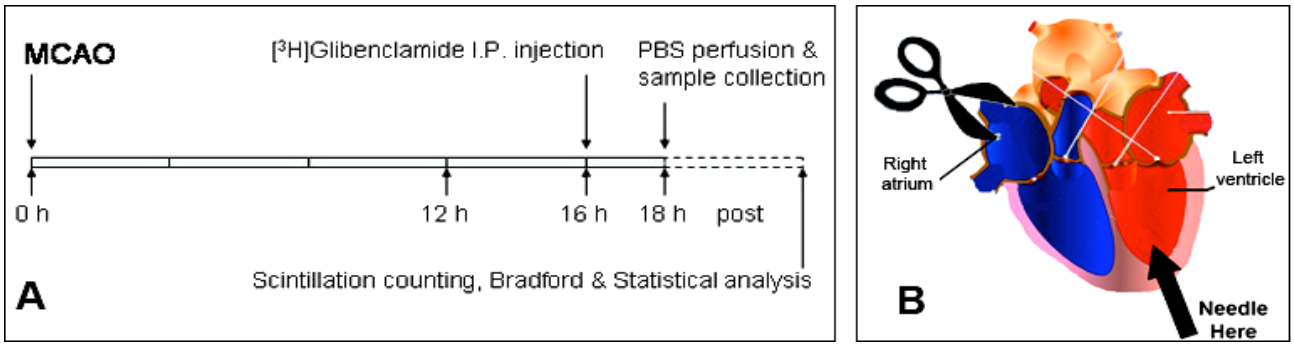

Fig. 3.3. A) Schematic protocol to calculate Gbc bioavailability. **B)** Illustration of transcardial perfusion pointing the insertion of the needle in the left ventricle and the incision in the right atrium.

3.4 Short-term glibenclamide effects: Dose-response study

To evaluate the effects of Gbc (Sigma-Aldrich, St Louis, MO) on tMCAO by means of functional, histological and immunohistochemical studies, we divided 60 animals into four groups (n= 15 /group). Each rat received three 0.2 ml injections of either 0.01 M PBS (pH 7.4), 0.02 µg, 0.2 µg, or 2 µg Gbc into the tail vein (in total, Gbc doses were 0.06 µg, 0.6 µg and 6 µg). Injections were given at 6, 12 and 24 h after reperfusion. Gbc was prepared in dimethylsulfoxide (DMSO) (Sigma-Aldrich, St Louis, MO) and diluted in 0.01 M PBS to the final concentration required for each group (DMSO final concentration <0.5%).

3.5 Long-term glibenclamide effects

For the long-term study, we divided 34 rats into the following three groups: sham rats (n=10), vehicle-treated MCAO rats (n=12) and Gbc-treated MCAO rats (n=12). Each rat received three injections of 0.2 ml of either 0.01 M PBS (pH 7.4) or 0.2 µg Gbc into the tail vein 6, 12 and 24 h after reperfusion (total dose 0.6 µg). Gbc was prepared in DMSO and diluted in 0.01 M PBS to final concentration (DMSO final concentration <0.5%).

3.6 Labeling of proliferating cells

In accordance with previous studies that fixed the proliferation peak from days 4 to 6 after MCAO (Arvidsson et al., 2002) and in order to analyze the long-term cell proliferation, we administered intraperitoneal injections of bromodeoxyuridine (BrdU; 50 mg/kg in PBS 50 mM) to 90 min tMCAO rats from postoperative days 4 to 8. MCAO groups were evaluated by measuring infarct volumes at the end of the study and unsuccessful transient MCAO animals were discarded from the study data (n = 2 from vehicle group).

3.7 Post-ischemic Motor and Behavioral Outcome Measures

Seven-point and 28-point neuroscore tests were used to assess post-ischemic motor and behavioral deficits, modified from (Zausinger et al., 2000). In brief, a blinded investigator conducted the neurological tests: pre-MCAO (baseline), 2, 24, 48 and 72 h after reperfusion (3 day follow-up groups).

3.7.1 The Seven-point scale was as follows:

Grade 6: Normal extension of both forelimbs towards the floor when lifted gently by the tail

Grade 5: Consistent flexion of the forelimb contralateral to the injured hemisphere, varying from mild wrist flexion and shoulder adduction to severe posturing with full flexion of wrist, elbow, and adduction with internal rotation of the shoulder.

Grade 4: Dysfunctional rats with a consistently reduced resistance to lateral push towards the paretic side.

Grade 3: Rats circling towards the paretic side if pulled and lifted by the tail.

Grade 2: Rats circling towards the paretic side if pulled by the tail.

Grade 1: Rats circling spontaneously towards the paretic side.

Grade 0: Rats with no spontaneous motion.

3.7.2 The 28-Point Scoring was as follows (parameters analyzed):

Paw placement (max. score 4)

Righting reflex (max. score 1)
Behavior on a horizontal bar (max. score 3)
Behavior on an inclined platform (max. score 3)
Contralateral rotation (max. score 2)
Visual forepaw reaching (max. score 2)
Circling (max. score 4)
Contralateral reflex (max. score 1)
Grip strength (max. score 2)
Motility (max. score 3)
General condition (max score 3)
The maximum score of a normal rat is 28 points.

The 28-point neuroscore test was broken down into sub-scores for subsequent analysis describing paw function (paw placement, horizontal bar, grip strength), general condition (motility, general condition, righting reflex, inclined platform) and turning preference (circling, contralateral reflex, contralateral rotation). At the same time-points, an individual body weight follow-up was performed. Animals with more than 25% of body weight loss were sacrificed.

3.8 Behavioral Outcome Measures

3.8.1 Limb-placing Test

The modified version of the limb-placing test was performed in baseline conditions and on postoperative days 2, 4, 7, 10, 13, 16, 19, 22, 26 and 29 (Puurunen et al., 2001). The animals were habituated for handling and testing before the induction of ischemia. The test included seven limb-placing tasks to assess the integration of forelimb and hindlimb responses to tactile and proprioceptive stimulation. Both sides of the body were tested to assess forelimb and hindlimb function. The following scoring was used: 2 points, normal response; 1 point, delayed and/or incomplete response; 0 points, no response. All tasks were scored by a tester blind to the treatment groups and performed as follows:

In the first task, the rat was suspended 10 cm over a table by the tail and the stretch of the forelimbs towards the table was observed. In the second task, the rat was positioned towards the table and its forelimbs were placed on the table. Each forelimb was gently pushed over and we measure rats' ability to retrieve their limbs. The third task was the same as the second one except that the rat's head was kept upward in a 45° angle without whiskers stimuli. Next, the rats were placed along the table edge to check for lateral placement of the forelimb (fourth task) and the hindlimb (fifth task). In the sixth task, the rat was again positioned towards the table with the hindlimbs just over the table edge. Each hindlimb was pulled down and gently stimulated by pushing towards the side of the table. In the seventh task, the forelimbs of the rat were on the edge of the table and the rat was gently pushed from behind toward the edge to assess forepaw resistance.

3.8.2 Forelimb Asymmetry Test

The cylinder test was used to assess imbalance between impaired and non-impaired forelimbs (Karhunen et al., 2003). Pretrained animals were tested in baseline conditions and on postoperative days 7 and 29. Briefly, the rats were placed in a Plexiglas cylinder (Ø 20 cm) for at least 4 min or until the rats were observed to rear a minimum of 20 times (**Fig. 3.4**). Sessions were videotaped from below the cylinder and analyzed using a video recorder with slow motion function to determine the number of contacts by both forelimbs and by either impaired or non-impaired forelimbs. The cylinder score for an impaired forelimb was calculated as: contralateral contacts/total contacts x 100 %.

3.8.3 Tapered/Ledged Beam-Walking Test

The sensorimotor function of hindlimbs was evaluated using a tapered/ledged beam (Zhao et al., 2005). Pretrained animals were tested in baseline conditions and on postoperative days 7 and 29. The beam-walking apparatus consisted of a tapered beam with underhanging ledges on each side to permit foot faults without falling and the end of the beam was connected to a black box, where the animals were allowed to rest for 1 min between trials (**Fig. 3.4**). Performance was videotaped and analyzed by calculating the slip ratio (number of slips/number of total steps) of the

impaired (contralateral to lesion) hindlimbs. Steps onto the ledge were scored as a full slip and a half-slip was scored when the limb touched the side of the beam. The mean of three trials was used for statistical analyses. An observer blind to the experimental groups performed all the behavioral analyses.

Fig. 3.4. Behavioral room where the Tapered Ledged Beam-Walking Test (left) and the Forelimb Asymmetry Test (right) were performed**.**

3.8.4 Morris Water-Maze

Spatial learning was assessed using a modified version of the Morris water-maze task (Puurunen et al., 2001). Rats were given four trials per day on postoperative days 27 to 29 followed by the probe trial without the platform. The pool (Ø 150 cm) was divided into four quadrants or three annulus zones of equal surface area. The starting locations were called north, south, east, and west, and were located arbitrarily at equal distances along the pool rim. The platform was located in the middle of the northeast quadrant 25 cm from the pool rim. The swim paths were monitored by a video camera connected to a computer through an image analyzer (HVS image). When the rat failed to find the hidden platform within 50 s, it was placed on the platform. The animal was allowed to remain on the platform for 10 s and to rest for 1 min after trials. The starting point was changed after each trial in the order described below. Escape latency (time to reach the platform) and the path length the animal swam to find the platform were parameters used to assess their performance in the water-maze task. Swimming speed (path length/escape latency) was calculated to exclude the effect of sensorimotor impairment. At the end of the

third testing day, a 30 s probe trial without the platform was used to evaluate how well rats remembered the location of the platform (passes over the previous platform location). Time spent in different annulus zones and quadrants of the pool was analyzed to examine the search strategies used by the animals.

	STARTING POINT				
	Trial 1	**Trial 2**	**Trial 3**	**Trial 4**	
Day 1	S	N	W	E	
Day 2	W	E	S	N	
Day 3	S	N	W	E	S*

* Denotes 30 s Probe Trial without the platform (N, north; S, south; E, east and W, west)

3.9 Imaging studies

Seventy-two hours after 60 min tMCAO, animals were deeply anesthetized with pentobarbital (60 µg/kg Mebunat, Orion Pharma, Finland). Then, T_2-weighted magnetic resonance imaging (T_2-MRI) was performed with a Varian Inova console interfaced to a 4.7 T horizontal magnet equipped with actively shielded gradient coils. A half-volume coil, driven in quadrature mode, was used for signal transmission and reception. To determine the cerebral infarct volume, T_2-weighted multislice (12-14 continuous slices) images were acquired by use of double spin-echo sequence with adiabatic refocusing pulses TR = 3 s, TE = 80 ms, 256x128 matrix size, 35x35 mm^2 FOV and a slice thickness of 1 mm.

Schematic of *In vivo* Study protocol:

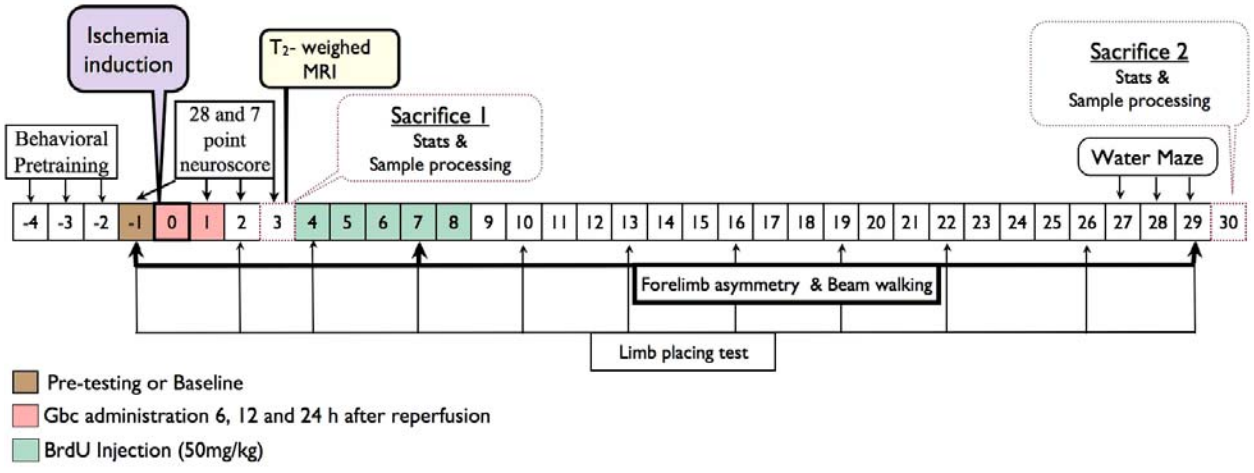

3.10 Histological and Immunohistochemical Procedure

After the MRI study, a group of animals (n=60) were anesthetized and perfused transcardially as described above, with heparinized saline (2.5 IU/ml) followed by 4 % w/v paraformaldehyde in 0.1 M phosphate buffer (PB, pH 7.4). Then brains were immersed in 4 % w/v paraformaldehyde in 0.1M PB for 24 hours, rinsed with 0.01 M PBS, cryoprotected in 30% w/v sucrose in PB for 2 days and frozen in liquid nitrogen-cooled isopentane. These brain specimens were stored at -80°C, until sectioning. Based on T_2-MRI results of the ischemic damage 72 h after reperfusion, the ischemic core was located at between -0.8 to -1.8 mm to Bregma (Paxinos and Watson 1986). A total of 60 serial sections/rat of 14 μm were collected with a cryotome, covering the entire brain.

Thirty days after MCAO, a second group of animals (n=34) were also anesthetized and transcardially perfused following the protocol described below. Brains were then post-fixed, cryopreserved in 30% w/v sucrose in PB for 2 days and frozen on dry ice. Sections (14 μm) covering the entire brain were cut with a cryotome.

3.10.1 Nissl and Haematoxylin-Eosin protocols:

Sections were used for Nissl standard and Haematoxylin-Eosin (H&E) staining. Sections stained with H&E were randomly selected to determine the total infarct volume using the optical microscope software AxioVision 4 AC (Zeiss) and applying the Cavallieri's principle. The total infarct volume was calculated by subtracting the area of the remaining tissue in the ischemic hemisphere from the area of the intact contralateral tissue of each section.

Protocol for Nissl staining:

1. Bring section to room temperature, (RT), 20 min, RT.
2. Place slides into chloroform (80 % v/v) + ethanol 95% (10 % v/v) + ether (10 % v/v) during 10 min, and then dehydrate through 95%, 100 % alcohol and xylene (5 min).
3. Rehydrate the samples through 100% and 95 % alcohol (5 min).
4. Stain in 0.1% cresyl violet solution (w/v) for 5-10 minutes.

5. Rinse quickly in distilled water (>1 min).
6. Dehydrate through 95% (2 min), 100 % alcohol (2 min) and xylene (>10 min).
7. Mount slides with DPX.

Protocol for Haematoxylin-Eosin staining:

1. Bring section to RT during 20 min.
2. Place slides into PBS (0.9 % w/v NaCl) 0.01M, pH 7.4 during 10 min.
3. Rinse into distilled water (H_2Od) for 2 min.
4. Stain with Mayer's Haematoxylin (Sigma-Aldrich) during 2 min.
5. Rinse in running tap water to reach desired color (8 min approximately).
6. Rinse in H_2Od during 3 min.
7. Stain with Eosin solution (0.5% w/v, Merk) in water during 5 min
8. Rinse in running tap water to reach desired color (8 min approximately).
9. Dehydrate through 70% (3 min), 95% (3 min), 100 % alcohol (3 min) and xylene (>10 min).
10. Mount slides with DPX.

3.10.2 Alizarin Red staining for calcium deposits:

To determine calcium deposits, sections were stained with the Alizarin red method (2% in 50 mM Tris/HCl, pH 7.6) and counterstained with fast green (0.5% in 50 mM Tris/HCl) as described elsewhere (Mahy et al., 1999; Rodriguez et al., 2004):

1. Bring section to RT during 20 min.
2. Rinse slides into 50 mM Tris/HCl, pH 7.6 for 2 min.
3. Stain with Alizarin Red (1 % w/v; Merk) in Tris/HCl 50 mM during 2 min.
4. Stain with Fast Green (0.2 % w/v) in Tris/HCl 50 mM during 30 seg.

5. Rinse in acetone during 10 min (x2)
6. Rinse in acetona:xylene (1:1) during 15 min.
7. Rinse in xylene during >10 min
8. Mount slides with DPX.

3.10.3 Fluorojade B staining for degenerating neurons:

Degenerating neurons were detected by Fluorojade B (FJB; Millipore, Billerica, MA) fluorochrome (Schmued et al., 1997), as follows. Sections mounted on 10% Poly-D-lysine slides were sequentially immersed in 1% NaOH in 80% ethanol for 5 min, 70% ethanol for 2 min, and distilled H_2O for 2 min. They were then transferred to 0.06% $KMnO_4$ for 10 min and rinsed in distilled H_2O. The staining solution was prepared from a 0.01% stock solution of FJB (1M), resulting in a final dye concentration of 0.0004%. After 20 min in the staining solution, the slides were rinsed in distilled H_2O, dried, and mounted with Prolong-Antifade (Invitrogen, Carlsbad, CA).

3.10.4 Immunohistochemical Procedures

Immunohistochemistry was carried out with the avidin-biotin peroxidase method as previously described (Rodriguez et al., 2009; Rodriguez et al., 2005).

General protocol for Immunohistochemistry:

1. Bring section to RT during 20 min.
2. Place slides into PBS (0.9 % w/v NaCl) 0.01M, pH 7.4 during 10 min.
3. For Endogen Peroxidase Inhibition place the slides into PBS 0.01M with 10 % (v/v) methanol and 0.03 % (v/v) H_2O_2 during 10 min.
4. Rinse slides into PBS 0.01M, pH 7.4 during 5 min (x3).
5. Add **Blocking Solution** (PBS – 0.3-0.5 % (v/v) Triton X-100 or Saponin, 5-10 % (v/v) normal serum and 5-10 % (v/v) bovine serum albumin (BSA) and incubate during 2-3 h, at RT and dark.
6. Add directly the primary antibody diluted in **Immunobuffer (**PBS

– 0.3-0.5 % (v/v) Triton X-100 or Saponin, 1 % (v/v) normal serum and 1 % (v/v) BSA, and leave it during 1 h at RT and dark. Then keep it overnight (O/N), at 4ºC and dark.

7. Bring section to RT during 1 h.
8. Rinse slides into PBS 0.01M, pH 7.4 during 5 min (x3).
9. Add the secondary antibody diluted in **Immunobuffer** (PBS – 0.3-0.5 % (v/v) Triton X-100 or Saponin, 1 % (v/v) normal serum and 1 % (v/v) BSA, incubate for 2-3 h, at RT and dark.
10. Rinse slides into PBS 0.01M, pH 7.4 during 5 min (x3).

10b. 10b. If the secondary antibody was biotin-conjugated, add ExtrAvidin®-HRPeroxidase (1:250; PBS 0,01M pH 7,4) for 2 h, at RT and dark, otherwise go to step 13.

11. Rinse slides into PBS 0.01M, pH 7.4 during 5 min (x3).
12. Rinse slides into 50 mM Tris/HCl, pH 7.6 for 10 min.
13. Place the slides into the Developing solution **(**50 mM Tris/HCl, pH 7.6 with 0.03 % (w/v) diaminobenzidine and 0.006% (v/v/ H_2O_2) and incubate for 5-15 min, at RT and dark, until desired color is reached.
14. Stop development placing slides into distilled water, 10 min (x2).
15. Dehydrate through 70% (3 min), 95% (3 min), 100 % alcohol (3 min) and xylene (5 min).
16. Rinse in xylene during >10 min.
17. Mount slides with DPX.

- Blocking Solution and **Immunobuffer** specifications for each antibody in detail in **APPENDIX I**.

- For IB4-HRP conjugated immunolabeling steps 9-12 were omitted.

- Steps with Blocking Solution or Immunobuffer were place into a humidifier chamber.

Proliferating cells were determined by labeling of the BrdU-positive cells. We used the mouse monoclonal anti-BrdU antibody (1:100; Sigma-Aldrich) and the biotin-conjugated rat anti-mouse IgG (1:150). ExtrAvidin-HRPeroxidase (1/250) was

used for detection. In this case, after cooling down the samples, we performed a pretreatment with HCl 1N + Formamide (50% v/v) (1:1) during 1 h at 40ºC. Then samples were rinsed in Borate buffer 0.1M (pH 8.5) for 10 min and transferred into PBS 0.01 M for 10 more minutes before continue with step 3.

Morphological and histological parameters were measured with the optical microscope software AxioVision 4 AC, (Zeiss) and analyzed by the Image Pro Plus v.5.1 image analysis system (Media Cybernetics Inc., Bethesda, MD, USA). Whole left hemispheres were studied on serial Nissl and H&E stained coronal sections, that allow to differentiate between structures and identify the damage to be accurately quantified. Initially cortical and subcortical regions were well delimited and analyzed separately (**Fig. 4.4**). As such, three different affected areas were considered in each region: first, a non-infarcted zone whose tissue architecture had avoided injury and was intact; second, a necrotic zone defined as the infarct nucleus showing few scattered cells stained by NeuN immunohistochemistry; and finally, the peri-infarcted zone was defined as the remaining zone between the non-infarcted and necrotic ones. In some cases, the peri-infarcted and necrotic zones were analyzed together and defined as the entire lesioned zone.

The areas of astrogliosis and microgliosis were measured on glial fibrilar acidic protein (GFAP)-immunostained and Isolectin B4 (IB4)-stained sections, respectively, with the same image analysis system. In all cases, the contralateral hemisphere area was measured in the same sections, to calculate the effects of histological procedures on tissue size, and correct for variability in individual brain size and tissue shrinkage.

Stereological methods were used to quantify the number of cells at the core of the lesion. We applied the optical fractionator's method to count labeled cells. Non-infarcted, peri-infarct and necrotic regions were outlined at cortical and subcortical levels at 2.5x magnification on arbitrary uniform random (AUR) coronal sections, located between -0.8 mm and -1.8 mm to Bregma **(Fig. 3.5**) (Paxinos and Watson 1986). Four sections of each animal were selected to visualize individual cells at 40x in AUR-sampled sites chosen by the Mercator Pro 7.0 software (ExploraNova, La Rochelle, France), and then counted.

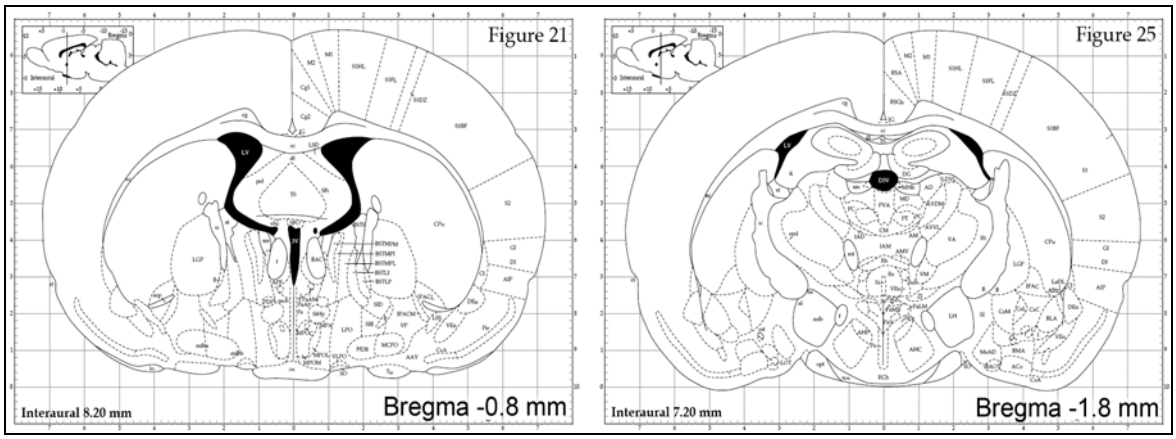

Fig. 3.5. Illustrative images at Bregma -0.8 mm and -1.8mm from Paxinos and Watso 1986.

3.11 Immunofluorescence

Double immunofluorescence labeling was carried out following the protocol described for immunohistochemistry but briefly changed. Hydrated samples were mounted on coverslips with Pro-long Antifade (Invitrogen, Carlsbad, CA) and slices were stored at 4ºC. Confocal images were acquired by a Leica TCS SL laser scanning confocal spectral microscope (Leica Microsystems Heidelberg GmbH, Mannheim, Germany) and image analysis was done with ImageJ 1.39u (National Institutes of Health, USA).

General protocol for Immunofluorescence:

1. Bring section to RT during 20 min.
2. Place slides into PBS (0.9% w/v NaCl) 0.01M, pH 7.4 for 10 min.
3. Add **Blocking Solution** (PBS – 0.3-0.5 % (v/v) Triton X-100 or Saponin, 5-10 % (v/v) normal serum and 5-10 % (v/v) BSA during 2-3 h, at RT and dark.
4. Add directly the primary antibody diluted in **Immunobuffer (**PBS – 0.3-0.5 % (v/v) Triton X-100 or Saponin, 1 % (v/v) normal serum and 1 % (v/v) BSA, and leave it during 1 h at RT and dark. Then keep it overnight (O/N), at 4ºC and dark.
5. Bring section to RT during 1 h.
6. Rinse slides into PBS 0.01M, pH 7.4 during 5 min (x3).

7. Add the secondary antibody diluted in **Immunobuffer** (PBS – 0.3-0.5 % (v/v) Triton X-100 or Saponin, 1 % (v/v) normal serum and 1 % (v/v) BSA, 2-3 h at RT and dark.
8. Rinse slides into PBS 0.01M, pH 7.4 during 5 min (x3).

8b. If the secondary antibody was biotin-conjugated, add ExtrAvidin®-FITC (1:250; PBS 0,01M pH 7,4) and incubate for 2 h at RT and dark, otherwise go to step 10.

9. Rinse slides into PBS 0.01M, pH 7.4 during 5 min (x3).
10. Mount slides with Pro-long Antifade (Invitrogen, Carlsbad, CA) store at 4ºC.

-Blocking Solution and **Immunobuffer** specifications for each antibody in detail in **APPENDIX I**.

-Controls for non-specific binding were performed excluding primary antibodies.

-Steps with Blocking Solution or Immunobuffer were place into a humidifier chamber.

The fate of the new proliferating cells was determined by double immunostaining with mouse monoclonal anti-BrdU antibody (1:100; Sigma-Aldrich), biotin-conjugated rat anti-mouse IgG (1:150) and antibodies against specific cellular specific markers, as described elsewhere (Valente et al., 2009). ExtrAvidin-FITC (1/250; Sigma-Aldrich) was used to detect BrdU-positive cells. For the other cellular markers, specific anti-IgGs from various species were used conjugated with AlexaFluo-555 (1:300; Invitrogen). Samples were also pretreated with HCl 1N + Formamide (50% v/v) (1:1) during 1 h at 40ºC, rinsed in Borate buffer 0.1 M (pH 8.5) for 10 min, and then transferred into PBS 0.01 M for 10 more minutes before continue with step 3.

Confocal images were acquired using a Leica TCS SL laser scanning confocal spectral microscope (Leica Microsystems Heidelberg GmbH, Mannheim, Germany) and images were analyzed with ImageJ 1.39u (NIH, USA).

3.12 Culture, morphology study and immunocytochemistry of BV2 microglia

BV2 cells (Cell Bank, Interlab Cell Line Collection, ICLC, Geneva) were cultured in RPMI 1640 medium with L-glutamine and supplemented with 10 % v/v heat-inactivated fetal bovine serum (FBS), 100U/ml penicillin and 100µg/ml streptomycin (Gibco, Carlsbad, CA). Cells were grown in a humidifier cell incubator containing 5% CO_2 at 37ºC. Before activation, cells were sub-cultured on 24-well plates at a density of $5x10^4$ cells/ml for 24 hours and then activated with lipopolysaccharide 0.1 µg/ml (LPS; Sigma-Aldrich, St Louis, MO) and IFNγ 0.05 ng/ml (Sigma-Aldrich, St Louis, MO), as described elsewhere (Saura et al., 2003).

A Gbc working solution was prepared in DMSO and diluted 1:50 (v/v) in culture medium. Cell cultures were pre-treated 30 minutes before or post-treated 24 hours after activation with LPS+IFNγ with either 1, 10^{-3} or 10^{-5} nM Gbc diluted in culture medium (DMSO final concentration <0.01%). A control group without activation but treated with 1 nM Gbc was added to each treatment-group. 48 hours after activation, culture media were collected for further analysis.

For immunocytochemistry assays, BV2 cells were grown on poly-D-lysine (Sigma-Aldrich, St Louis, MO) coated sterile coverslips and the medium was changed on day of activation with LPS+IFNγ. At 48 hours, cells were fixed in ice-cold methanol for 30 seconds and then blocked with 5% (w/v) normal serum and 5 % (w/v) BSA diluted in PBS 0.01M (pH 7.4). For immunodetection we used mouse anti-CD11b (1:300), goat anti-SUR1 (1:100), rabbit anti-Kir6.1 or anti-Kir6.2 (1:400) as primary antibodies and we detected them with anti-mouse AlexaFluor-555 or anti-rabbit/-goat AlexaFluor-488 conjugated secondary antibodies (1:500), as described above for immunofluorescence. Controls for non-specific binding were performed excluding primary antibodies. Cell nuclei were stained with Hoescht33258 (0.5µg/ml in PBS; Invitrogen, Carlsbad, CA). Coverslips were mounted with Pro-long Antifade (Invitrogen, Carlsbad, CA) and slides were stored at 4ºC.

For cell morphology analysis, direct immunofluorescence was carried out with anti-alpha-tubulin FITC conjugated as primary antibody (1:500), in which 5 random pictures/well were taken by a Leica DMI 6000B inverted microscope equipped with LAS AF Leica software (Leica Microsystems Heidelberg GmbH, Mannheim,

Germany). In each picture, the area and perimeter of every individual cell were measured by ImageJ 1.39u (National Institutes of Health, USA).

To study their phagocytic capacity, cells were incubated for 2, 5, 15 and 30 minutes at 37ºC in the presence of 2µm diameter FluoSpheres carboxylate microspheres (F-8826; Molecular Probes) at 0.01% solid mass, as described elsewhere (Saura et al., 2003). In parallel, immunofluorescence with anti-alpha-tubulin antibody conjugated with FITC was employed for cell identification as described above. To analyze phagocytic capacity, 5 random pictures/well were taken and cells containing at least one FluoSphere were counted in each picture. Results are given as a percentage of the total number of cells per well.

Schematic of *In vitro* Study protocol for BV2 cells:

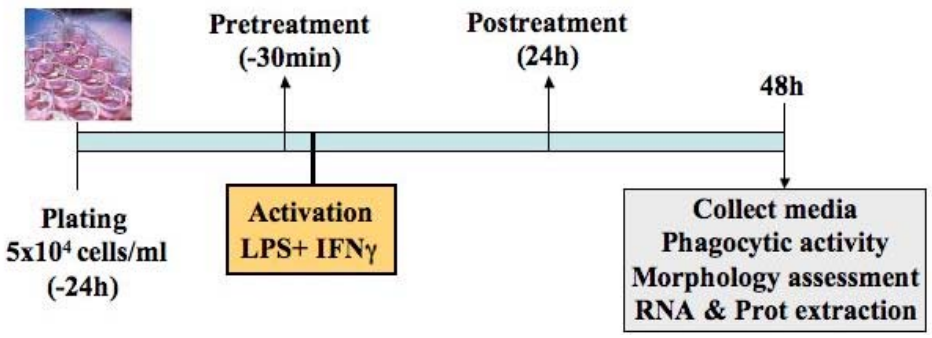

3.13 RT-PCR and Western blotting of K_{ATP} channel components in BV2 cells

RT-PCR was performed to assess the presence of SUR1, Kir6.1 and Kir 6.2 mRNA in BV2 cells. Roche Diagnostics (TIB-MOLBIOL, Berlin, Germany) synthesized the primers for RT-PCR analysis. Total RNA from BV2 cells was isolated using NucleoSpin RNA/protein kit in line with the manufacturer's instructions (Macherey-Nagel, Germany). The concentration of total RNA isolated was quantified by a NanoDrop N1000 spectrophotometer (Thermo, Wilington, DE). Specific primers were designed against mouse mRNA sequences (Genbank Accession numbers in brackets) of Kir6.1 (NM_008428.4), Kir6.2 (NM_010602.2), SUR1 (NM_011510.3), SUR2A (D86037) and SUR2B (D86038) as described elsewhere (Morrissey et al., 2005) and sequence of 18S non-coding mRNA (NR_003278.1) was used as control (**Table 1**). RT reactions were carried out using random primers and 2 µg of mRNA with the

AffinityScript Multiple Temperature cDNA Synthesis kit (Stratagene, CA). PCR was performed with the Taq PCR Core kit from Qiagen (Studio City, CA), using 2µl of RT reaction as a template. The reaction components and cycling conditions for Kir6.1, Kir6.2, SUR1 and SUR2A/B are described in detail (for detail **APPENDIX II**). For 18S mRNA, cycling conditions had the annealing temperature fixed at 57ºC in line with the manufacturer's instructions. Appropriate templates were included as positive and negative controls. PCR products (10 µl) were separated by 1.5% agarose gel electrophoresis at 100V and viewed by staining with ethidium bromide.

Table 1- Primer sequences used for RT-PCR.

Species	Size (bp)	Primer	Sequence
Kir6.1	297	F	5′-ACCAGAATTCTCTGCGGAAG-3′
		R	5′-GCCCTGAACTGGTGATGAGT-3′
Kir6.2	312	F	5′-TTGGAAGGCGTGGTAGAAAC-3′
		R	5′-GGACAAGGAATCTGGAGAGAT-3′
SUR1	217	F	5′-GCCTTCGTGAGAAAGACCAG-3′
		R	5′-GAAGCTTCTCCGGTTTGTCA-3′
SUR2A/B	SUR2A: 397	F	5′-ATCATGGATGAAGCCACTGC-3′
	SUR2B: 221	R	5′-AACGAGGCAAACACTCCATC-3′
18S	488	F	5′-TCAAGAACGAAAGTCGGAGG-3′
		R	5′-GGACATCTAAGGGCATCACA-3′

F and **R** referred to forward and reverse primers respectively.

Whole-cell culture proteins were obtained in buffer containing a cocktail of protease inhibitor (RIPA) (Santa Cruz Biotechnology, Santa Cruz, CA) and brain homogenates, as described elsewhere (Acarin et al., 2000). Briefly, brain samples were homogenized in ice-cold Tris/HCl 50 mM (pH 7.4) buffer containing RIPA and using a potter homogenizer. The homogenates were centrifuged for 10 min (45000 g., 4ºC), and then the pellet was resuspended in Tris/HCl 50 mM (pH 7.4) and repeat the same procedure with potter homogenizer and the centrifuge twice. At the end, the pellet was collected and resuspended in lysis buffer containing (20 mM Tris/HCl pH 7.5, 1% (v/v) Triton X-100, 1 mM EDTA, 2 mM DTT, 120 mM NaCl, 50 mM KCl).

The obtained solutions were collected and the Bradford method was used to calculate the protein content of each sample (Bradford 1976). Aliquots containing 15 µg protein were subjected to 10% SDS-PAGE in Running buffer (glycine 1.92 M, Tris 0.25 M, 0.1% w/v SDS). The gel was running during 20 min at 80V and then the voltage was increased to 100V. Proteins were then transferred to Nitrocellulose membrane (Amersham Pharmacia Biotech, San Francisco, CA) in Transfer buffer (Tris 0.12 M, glycine 0.027 M, 20 % v/v methanol) during 1h at 100V and at 4ºC. Membranes were probed by incubation with anti-SUR1 (1:100), anti-Kir6.1 and anti-Kir6.2 (1:500) as primary antibodies and with peroxidase-conjugated IgG as secondary antibody (1:2500) following the protocol described in the table below.

General protocol for Western-Blotting:

1. Place nitrocellulose membranes into tris-base saline buffer (TBS; 20 mM Tris-base, 134 mM NaCl, pH 7.4) with 0.1 % (v/v) Tween-20 (TBST) during 10 min (x2)
2. Add **Blocking Solution** (TBST, 5% (w/v) non-fat dry milk (NFDM) and 1 % (w/v) BSA during 1 h in a rotator shaker.
3. Add directly the primary antibody diluted in **Immunobuffer** (TBST, 5% (w/v) non-fat dry milk (NFDM) and 1 % (w/v) BSA, and leave it overnight (O/N) in a rotator shaker, at 4ºC and dark.
4. Rinse membranes into TBST during 5 min (x3).
5. Add the secondary antibody-HRPeroxidase conjugated diluted in **Immunobuffer** (TBST, 5% (w/v) non-fat dry milk (NFDM) and 1 % (w/v) BSA and incubate for 2 h at RT and dark.
6. Rinse membranes into TBST during 5 min (x3).
7. Rinse membranes into TBS during 10 min.
8. Develop membranes.

Blots were viewed by the enhanced chemiluminescence's system ECL-Plus, according to the manufacturer's instructions, and exposed to X-ray film (Amersham Pharmacia Biotech, San Francisco, CA). For band quantification, intensities were measured by ImageJ 1.39u (National Institutes of Health, USA).

3.14 Quantification of NO and TNFα production by BV2 cells

NO production was assessed in culture supernatants by the Griess reaction, a colorimetric assay that detects nitrite (NO^{2-}) as a stable reaction product of NO with molecular oxygen (Green et al., 1982). Briefly, we centrifuge the samples at 9000 r.p.m. to spin down the cells potentially present in the media, then, in a 96-well plate 50 µL of each sample was added to the well and incubated with 25 µL of Griess reagent A (1% sulfanilamide, 5% phosphoric acid) and 25 µL of Griess reagent B (0.1% N-1-naphthylenediamine) for 5 min. We measured the optical density of the samples at 540 nm with a microplate reader (Sunrise-Basic Reader, TECAN). The nitrite concentration was determined from a sodium nitrite standard curve ($NaNO_2$, 100 - 0µM).

We used an ELISA murine TNFα kit (PeproTech; London, UK) to determine the amount of TNFα released in the cell culture supernatants, and following the manufacturer's guidelines. Briefly, the capture antibody (1µg/mL) was incubated overnight in a 96-well plate, and then washed three times with Wash buffer (0.05 % v/v Tween-20 in PBS pH 7.2). Afterwards, the plate was incubated for1 h at RT with 300µL of Block buffer (1% w/v BSA in PBS), and then we washed (x3). A 50µL of sample or standard were added in each well and incubated for at least 2h, and then we washed the plate (x3). We added 100µL/well of the detection antibody (0.25µg/mL) and incubated at RT form 2h, and then we washed the plate (x3). For detection, 100µL of avidin-HRPeroxidase conjugated (1:2000) was added to each well and incubated 30 min at RT. To finish, 100µL of ABTS liquid substrate was added to each well and we incubated at RT while monitoring the color development with a microplate reader (Sunrise-Basic Reader, TECAN) at 405nm and a correction wavelength set at 650nm.

3.15 Primary Microglia Culture

Cell culture procedures were approved by the Ethics Committee of the *Universitat de Barcelona*, in accordance with the regulations established by the Catalan autonomous government (*Generalitat de Catalunya*). Primary glial cultures were obtained following the protocol described elsewhere Saura et al. (2003) but briefly

changed. Mixed glial cultures from 2- to 4-day-old Wistar rats or 2-4 C57BL/6 mice were obtained from cerebral cortex and digested with 0.25% trypsin-EDTA solution (Invitrogen) for 30 min at 37ºC. Trypsinization was stopped by adding an equal volume of culture medium, consisted in Dulbecco's modified Eagle medium-F-12 nutrient mixture (DMEM:F12, Invitrogen) supplemented with 10% FBS, 0.1% penicillin-streptomycin (Invitrogen), 0.5 mg/mL amphotericin B (Fungizone®, Invitrogen), and 0.04% deoxyribonuclease I (Sigma-Aldrich). Cells were pelleted (8 min, 1000 rpm), resuspended in culture medium, and brought to a single cell suspension by pipetting vigorously and filtering through a 105 mm-pore mesh. Cells suspension were seeded at a density of $3 \cdot 10^5$ cells/mL and grown in a humidifier cell incubator containing 5% CO_2 at 37ºC. Medium was replaced every 7 days. To verify the purity of microglial culture, cells were fixed with 4% paraformaldehyde for 15 min at 4ºC and immunocytochemistry was carried out with mouse anti-rat CD11b antibody (OX-42 clone, 1:500) and goat anti-mouse AlexaFluor-555 as a secondary antibody (1:500). The purity of the cultures was 98±1% (n = 5 cultures) as based on the number of CD11b positive cells.

To assess the effect of astrocytes on neurospheres (n = 5 cultures), half of the wells were processed as mixed-glial culture and half were processed to obtain pure-microglial cultures using the mild trypsinization method after 19–21 days in vitro (DIV). Briefly, mixed glial cultures were treated for 30-60 min with 0.06% trypsin-EDTA solution until the astrocyte layer is floating, then the same amount of medium with FBS is added to stop the reaction. After 2 washes with NeuroCult NSC basal medium, cells were cultured for 24 h on completed medium.

3.16 Sulfonylurea Receptor localization using Gbc-BODIPY-FL®

Rat primary microglial cultures were activated and treated 24 h after isolation as described below. Cells were activated with 0.1 mg/mL of recombinant LPS and 0.05 ng/mL of recombinant mouse IFNγ (Sigma-Aldrich). Cell cultures were then treated with Gbc diluted in culture medium at different doses (DMSO final concentration <0.05%) 30 min before activation with LPS+IFNγ. After 48 h, cells were incubated for 30 min at 37ºC in Hank's Buffered Salt Solution and supplemented with 500 nM Gbc–BODIPY-FL (green fluorescent dye; Invitrogen). After cell fixation with 4% w/v

paraformaldehyde, we performed immunocytochemical analyses with mouse anti-rat CD11b (1:500) antibody and goat anti-mouse AlexaFluor-555 as a secondary antibody (1:500). Cultures were directly observed in an AxioObserver Z1 (Carl Zeiss; GmbH, Germany) inverted microscope equipped with FluoUp and CoLoc image software (ExploraNova, La Rochelle, France) and recorded on a high sensitivity camera (RetigaEXi Fast 1394, QImaging). Image processing was using the method described by Jaskolski et al. (Jaskolski et al., 2005), which determine the labeling colocalization. The purity of the cultures was 97±1% (n = 4 cultures), as based on the number of CD11b-positive cells.

3.17 Neurosphere culture.

Adult mice were sacrificed by cervical dislocation, and the brains removed immediately to Petri dishes containing HEPES-buffered minimum essential medium (HEM), consisting of minimum essential medium (Invitrogen), supplemented with 16 mM HEPES (Sigma-Aldrich) and 100 U/ml penicillin/streptomycin (Invitrogen). The SVZ or hippocampus was dissected. Briefly, the tissues were minced and digested with 2mg/ml of Papain (SVZ) (Worthington) or 0.05% trypsin–EDTA (hippocampus) (Invitrogen) and incubated at 37°C for 7 min (SVZ) or 14 min (hippocampus), followed by the addition of 0.014% (w/v) trypsin inhibitor (type I-S from soybean; Sigma-Aldrich) dissolved in HEM (SVZ) or the equivalent volume of media (hippocampus). Following centrifugation at 100g relative centrifugal force (rcf) for 7 minutes, the resulting pellet was resuspended in 500 µl of 0.1 M PBS (calcium and magnesium free; Gibco/Invitrogen) and mechanically triturated into a single cell suspension. The cells were washed completed media consisted of: mouse NeuroCult neural stem cell (NSC) basal medium, 10% of mouse NeuroCult NSC proliferation supplements (Stem- Cell Technologies), 2% BSA (Roche), 2 µg/ml heparin (Sigma-Aldrich), 20 ng/ml purified mouse receptor grade EGF (BD Biosciences), and 10 ng/ml recombinant bFGF (Roche). They were then plated in 96-well plates, and cultured in 200 µl/well of completed medium in a humidified incubator at 37°C.

Potassium Chloride (KCl) acts as an activator of neural precursor cells proliferation (Walker et al., 2008), and the neurosphere growth medium already

contained 4.18 mM KCl. Therefore, for the depolarization experiments, additional KCl was added to give the appropriate final KCl concentration of 15 mM. The number and size of the SVZ neurospheres were determined 7 d after plating, whereas hippocampal neurospheres were assessed after 14 d.

3.18 Fluorescence-activated cell sorting and generation of primary neurosphere cultures.

Adult brains (3–4 month old) from the eGFP–Csf1r transgenic mice, were collected as described above and dissected into specific regions (SVZ and cortex). To assess the effect of Gbc on in neurosphere cultures in presence or absence of microglial cells, three different approaches were used: (1) SVZ dissected tissue was passed through the FACS but all cell populations was collected, which contains microglial cells (+MO), and plated in 200 µl/well of completed medium. (2) GFP^+ cells from the SVZ dissected tissue were separated and discarded by fluorescence-activated cell sorting (FACS) using a FACS Vantage cell sorter (BD Biosciences). The remained neurosphere culture, without microglial cells (-MO), was plated in 200 µl/well of completed medium. (3) SVZ dissected tissue was passed through the FACS but all cell populations was collected and plated in 100 µl/well of completed medium. Cortical GFP^+ cells were separated and collected by a FACS Vantage cell sorter (BD Biosciences) and counted with a hemocytometer. Then, 100 µl of the GFP^+ cell suspension was added over the neurosphere culture to a final ratio of to a final proportion of 40-cell-positive to 1-cell-negative, achieving an enriched-microglial culture (Enriched-MO). Primary cells were incubated for 7 d in humidified 5% CO2 to permit neurosphere formation, were the number and size of the SVZ neurospheres were determined.

To obtain microglial-conditioned media, cortical GFP^+ cells were collected by a FACS Vantage cell sorter (BD Biosciences) and harvested in a 15 mL falcon tubes to a final concentration of 100000 cells/mL.

3.19 Differentiation of primary neurospheres.

Neurospheres established from the SVZ and hippocampus were plated onto glass coverslips coated with poly-L-ornithine (Sigma) and laminin (natural mouse;

Invitrogen) in neurosphere differentiation medium containing mouse NeuroCult NSC basal medium, 10% mouse NeuroCult NSC proliferation supplements, and 100 U/ml penicillin/streptomycin (Invitrogen). To quantitatively analyze the multipotentiality of the neurospheres, individual neurospheres were selected from cultures. Neurospheres were allowed to differentiate for 6 d in a 5% CO2/ 37°C tissue culture incubator. The differentiated neurospheres were then analyzed for the acquisition of differentiation markers by immunohistochemistry, as described below.

3.20 Immunofluorescence of differentiated neurospheres.

To assess the differentiation potential of undissociated neurospheres, coverslips containing the neurospheres were rinsed gently with PBS and fixed with 4% paraformaldehyde for 15 min at 4ºC. The neurospheres were then rinsed three times with PBS to remove the PFA, and the fixed neurospheres were incubated in blocking solution (5% FCS and 5% normal goat serum in PBS containing 0.1% Triton X-100) for 1 h at 37°C, after which the blocking solution was replaced with fresh solution containing anti-beta-III-tubulin mouse IgG monoclonal antibody (diluted 1:2000; Promega) and incubated overnight at 4°C. The neurospheres were rinsed in PBS and then incubated for 30 min at 37°C in blocking solution containing Alexa Fluor 488-conjugated anti-mouse antibody (1:1000; Invitrogen). After washing with PBS, the slides were coverslipped with fluorescence mounting medium (Dako).

To count the number of beta-III-tubulin-positive cells in differentiated neurospheres, all neurospheres were selected. Data were expressed as a neurosphere containing <25, 25-100, 100-200 or >200 beta-III tubulin-positive cells/neurosphere.

3.21 Microglia activation and glibenclamide treatments.

To assess the effect of Gbc directly on hippocampal and SVZ neurosphere cultures, as well as, KCl activated neurosphere cultures, we add Gbc on the range from μM to fM at plating.

In order to characterize whether the blockade of the microglial K_{ATP} channel instructs SVZ neurogenesis, we performed primary neurosphere cultures with or without microglia (-MO, +MO and enriched-MO) were activated with 0.1 mg/mL of

LPS (Sigma-Aldrich) and 0.05 ng/mL of IFNγ (R&D), diluted in completed culture media at plating. FACS isolated GFP^+-microglial cells were activated when plating into the 15 mL falcon tubes, and 24 hours later conditioned-microglial media was collected to perform a new neurosphere assay and analyzed the cytokine levels as described below. Whereas, primary mixed-glial or primary microglial cultures were activated and treated 24 hours after the addition of completed medium in presence of LPS+IFNγ. At the same time, all cultures were co-treated with fresh Gbc solution, which was diluted in completed culture media and added until desired final concentration was achieved (DMSO final concentration <0.05%). The K_{ATP}-channel agonist Diazoxide 50μM, (Virgili et al., 2011) was added to the plate alone or in combination with Gbc.

3.22 Neuronal culture.

To assess the putative neuroprotection in presence of Gbc, embryonic neuronal culture from E16-E18 C57BL/6 mice were obtained from hippocampus and digested with 0.05% trypsin-EDTA solution (Invitrogen) for 15 min at 37ºC. Stop digestion adding the same volume of trypsin-inhibitor (Invitrogen) and spun for 5 min at 104 g. Discard supernatant and add 1 ml of DMEM:F12 media (Gibco), and then triturate cell suspension through a 19 gauge and a 23 gauge needle. Filter cells with a 40 μm diameter mesh and plate out onto glass coverslips coated with poly-L-ornithine (Sigma) to a final density of 100000 cells/well. At the same time, all cultures were co-treated with fresh Gbc solution, which was diluted in completed culture media and added to reach final concentration (DMSO final concentration <0.05%). The media supplemented with Gbc was changed after 24 hours. Immunofluorescence was carried out after 7 DIV as described before for differentiated neurosphere cultures. To count the number of beta-III tubulin-positive cells slides were mounted with fluorescence mounting media (Dako) with DAPI (0.5μg/ml; Invitrogen) to label nuclei. We took 5 random pictures/well by a Zeiss inverted microscope, and all beta-III-tubulin-positive cells were analyzed.

3.23 Cytometric Bead Array (CBA).

In order to quantify concentration of releasing cytokines in microglia-conditioned media, interleukins IL-6, IL-10, IL-12p70, IFNγ, TNFα and CCL2/MCP-1 were assayed using cytometric bead array (CBA) reagents (BD Biosciences) with four-color FACS Calibur flow-cytometer (BD Biosciences). In CBA, different bead populations with distinct fluorescence intensities had been coated with capturing antibodies specific for different cytokines/chemokines. After incubation with 50 μL of conditioned-microglial medium, the cytokine/chemokine-captured beads were mixed with phycoerythrin-conjugated detection antibodies to form sandwich immune-complexes. Fluorescence flow-cytometry of the beads provides simultaneous quantification of a panel of cytokines/chemokines.

3.24 Statistical Analysis

For Results Block I: Q-Q plots were calculated to test the normal distribution of data and variance homogeneity was checked by Levene's test. Most analyses were performed by one-way analysis of variance (ANOVA) followed by the post-hoc least significant difference test to compare differences between groups. When normality was not reached, the non-parametric Kruskal-Wallis (KW) test and then the Mann-Whitney U test were used to compare values for all groups. For the study of the blood-brain-barrier breakdown, standard deviation and mean values between control and ischemia brain tissue were compared with the F-test and Student-t tests respectively.

For the analysis of Neuroscore and MRI, differences among means were analyzed by one-way ANOVA followed by Dunnett's post hoc test (comparison with the vehicle treated group) or by the non-parametric KW test (between groups). Additional within group analyses were performed after original data analysis by using linear mixed models to fit data in which the rat was considered as a random effect. An autoregressive error was added into the model to control the time course of each parameter. The significance of the treatment, time and treatment by time effects was tested using the F-Wald test (Brown and Prescott 1999). The post-hoc paired differences of means were evaluated by correcting the type-I error rate

(Edwards and Berry 1987) to guarantee an overall type-I error rate of 5%.

To evaluate morphological and histological results, a double-blind method was used. Original data of area sizes were corrected by control of non-injured area sizes to minimize the effects of tissue sectioning deflection. Differences among means were analyzed by multifactor-ANOVA followed by the LSD post-hoc test. To correct for brain size variability, the whole hemisphere area size was used as covariate. To avoid misinterpretation of results, variance components were also analyzed in all cases. Only data from animals surviving until the end of the study were included in the statistical analysis. *In vitro* differences between means were analyzed by using one-way ANOVA followed by the LSD post hoc test.

All values are given as mean ± standard deviation (SD) or standard error of mean (SEM). Values of $p<0.05$ where considered significant. Analyses were performed with the Statgraphics 5.0 (STSC Inc., Rockville, MD) and StatsDirect (StatsDirect Ltd Altrincham, UK) statistical packages.

For Results Block II: Statgraphics 5.0 (STSC Inc., Rockville, MD) and GraphPad Prism4 (La Jolla, CA, USA) statistical packages were used. Differences in the limb-placing scores between experimental groups were analyzed by the Mann-Whitney U-test. We used the analysis of variance for repeated measures (MANOVA) to analyze the beam-walking, cylinder and water-maze data for the overall group effect. Groups were then compared using one-way analysis of variance (ANOVA) followed by a post hoc test (LSD). Probe trial data were tested by ANOVA followed by LSD. *In vitro* and histological data and differences in the infarct volumes between vehicle controls and Gbc-treated MCAO rats were analyzed using ANOVA followed by LSD. When normality was not reached, we applied the Kruskall-Wallis test followed by the Mann-Whitney *U*-test. All values are presented as mean ± standard error of mean (SEM). P values <0.05 were considered significant.

For Results Block III: Results were subjected to statistical analysis using the statistical software Prism (Graphpad). Experiments were subjected to statistical analyses using one-way or two-way ANOVA with significance determined at p values <0.05, followed by the Bonferroni *post hoc* test for group comparisons.